

Efficient optical cat state generation using squeezed few-photon superposition states

Haoyuan Luo^{1,2,*} and Sahand Mahmoodian^{1,3,†}

¹*Centre for Engineered Quantum Systems, School of Physics,
The University of Sydney, NSW 2006, Australia*

²*Sydney Quantum Academy, Sydney, NSW, Australia*

³*Institute for Photonics and Optical Sciences (IPOS),
School of Physics, The University of Sydney, NSW 2006, Australia*

Optical Schrödinger cat states are non-Gaussian states with applications in quantum technologies, such as for building error-correcting states in quantum computing. Yet the efficient generation of high-fidelity optical Schrödinger cat states is an outstanding problem in quantum optics. Here, we propose using squeezed superpositions of zero and two photons, $|\theta\rangle = \cos(\theta/2)|0\rangle + \sin(\theta/2)|2\rangle$, as ingredients for protocols to efficiently generate high-fidelity cat states. We present a protocol using linear optics with success probability $P \gtrsim 50\%$ that can generate cat states of size $|\alpha|^2 = 5$ with fidelity $F > 0.99$. The protocol relies only on detecting single photons and is remarkably tolerant of loss, with 2% detection loss still achieving $F > 0.98$ for cats with $|\alpha|^2 = 5$. We also show that squeezed θ states are ideal candidates for nonlinear photon subtraction using a two-level system with near deterministic success probability and fidelity $F > 0.98$ for cat states of size $|\alpha|^2 = 5$. Schemes for generating θ states using quantum emitters are also presented. Our protocols can be implemented with current state-of-the-art quantum optics experiments.

Introduction.—Efficiently generating high-fidelity, large-photon-number non-Gaussian states of propagating photons remains an outstanding problem in quantum optics. The optical Schrödinger cat state, a superposition of opposite amplitude coherent states $|\text{cat}_{\alpha,\pm}\rangle \propto |\alpha\rangle \pm |-\alpha\rangle$, is a particularly sought after non-Gaussian state as it forms a building block to generate other more complex non-Gaussian states such as the Gottesman-Kitaev-Preskill (GKP) state [1]. The GKP state has been proposed as a candidate for encoding qubits in fault-tolerant quantum computing and can be generated by ‘breeding’ squeezed cat states [2, 3]. Large-amplitude cat states are therefore considered to be a critical resource state for photonic quantum computing [4–14].

Since cat states are non-Gaussian bosonic states, their generation requires either a non-Gaussian input state [15–18], or they require Gaussian input states undergo non-Gaussian evolution [19, 20]. The latter requires a strong optical nonlinearity, posing a significant experimental challenge. Common approaches rely on using photon-number detection as a nonlinearity to perform photon subtraction on squeezed vacuum [21–26]. Photon subtraction protocols usually involve interfering photons using linear optics [27, 28], however, the success probability of generating cat states of large amplitudes is hindered by the conditional nature of these protocols. To tackle this high degree of non-determinism, alternative protocols involving multiple stages of photon subtraction were proposed [14, 29], resulting in near-deterministic cat state generation. However, the output fidelity is highly sensitive to detector efficiencies [14] and the cat state sizes produced in Ref. [29] are probabilistic.

In this paper, we propose interfacing few-photon superposition states, that can be generated rapidly by

quantum emitters, with squeezing to efficiently generate high-fidelity cat states. Single-photon sources have matured greatly in recent years and emitters such as quantum dots and atoms coupled to cavities can efficiently produce high-quality single photon states [30, 31]. We propose using quantum emitters to deterministically generate superpositions of zero and two photons $|\theta\rangle = \cos(\theta/2)|0\rangle + \sin(\theta/2)|2\rangle$. These resource states are already non-Gaussian, but have limited photon number and become poor approximations for larger cat states [32, 33]. In order to use these to produce cat states we consider squeezing the state with up to 10 dB of squeezing and performing a photon-subtraction protocol. Here, we present two photon-subtraction protocols. Our first protocol, shown in Fig. 1(a), uses two squeezed θ states and implements photon subtraction using linear optics. For the second protocol, shown in Fig. 1(b), we only require a single squeezed θ state and photon subtraction is implemented using a two-level system (TLS). We show that the use of a θ state as an input, as opposed to a Fock state, enables having a simultaneously high success probability and high fidelity, something that squeezed two-photon Fock state inputs cannot produce. Although our protocols require in-line squeezing, they otherwise provide balance of minimising experimental resources, while having high success probability $P_{\text{succ}} \gtrsim 50\%$ and produce cat states with $|\alpha|^2 > 4$ with fidelity $F > 0.99$.

θ states.— Since cat states are supported on either the even or odd number basis, for any photon subtraction protocol, one must fix the parity of the supported number basis of the resource state. The squeezing operator, defined as $\hat{S}(r) = e^{-\frac{r}{2}(\hat{a}^2 - \hat{a}^{\dagger 2})}$ with squeezing strength $r \in \mathbb{R}$, preserves the parity of any particular number state. This reasoning underlies the use of squeezed vacuum and photon subtraction to generate cat states. Since

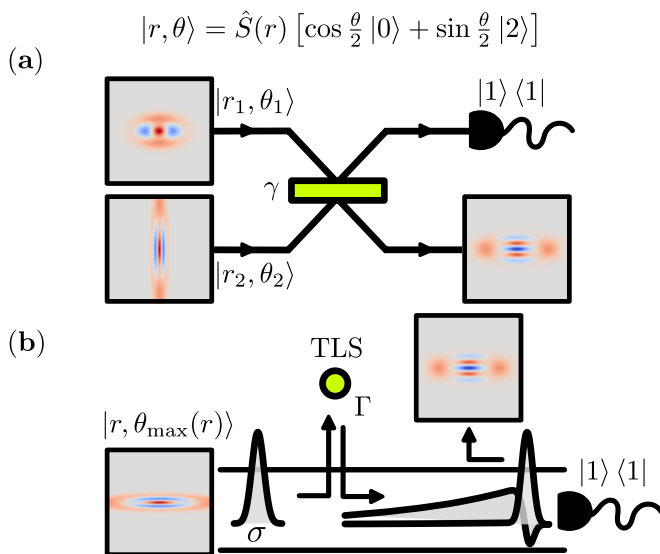


FIG. 1. Schematics of linear (a) and nonlinear (b) single-photon subtraction schemes for cat state generation. (a) Two resource states, parameterized by their squeezing strengths r_i and angles θ_i , are used as inputs into a beamsplitter with transmission and reflection coefficient $\cos \gamma$ and $i \sin \gamma$, respectively. Conditioned on a single-photon detection in the top output channel, a cat state is prepared in the bottom channel. (b) A resource state with $\theta_{\max}(r)$ chosen, such that the mean photon number is maximized under squeezing r , is prepared in a Gaussian wave packet with width σ and scatters off a two-level system (TLS) that is chirally coupled to the waveguide with coupling strength Γ . After scattering, the most dominant mode is extracted using a quantum pulse gate. Detecting a single-photon in the leftover modes heralds a cat state in the dominant mode. The input and output states are depicted using their Wigner functions. After unsqueezing (not shown) the output states here are approximate cat states of size $|\alpha|^2 = 4$.

we propose using quantum emitters to deterministically generate resource states, we seek to take advantage of a squeezed superposition of vacuum and two-photon Fock state, namely

$$|r, \theta\rangle = \hat{S}(r) \left[\cos \left(\frac{\theta}{2} \right) |0\rangle + \sin \left(\frac{\theta}{2} \right) |2\rangle \right], \quad (1)$$

where $\theta \in [0, 2\pi)$. These types of states were first considered in [32, 33]. The suitability of $|r, \theta\rangle$ for approximating cat states can be understood in terms of the stellar rank or the core-state expansion [20, 34, 35]. Gaussian states have zero stellar rank and Gaussian processes do not change the stellar rank of a state. On the other hand, non-Gaussian states such as cat states have infinite stellar rank. Nevertheless, such non-Gaussian states can be well approximated by squeezing a finite superposition of Fock states, which itself has a finite stellar rank. The quality of this approximation improves as the Fock state superposition is truncated at higher values, i.e., by squeezing a state with a larger stellar rank. The

state in Eq. (1) can therefore be made to better approximate larger Schrödinger cat states after undergoing a non-Gaussian process such as photon subtraction.

Linear photon subtraction.—We propose using squeezed θ states as inputs for generalized linear photon subtraction (see Fig. 1(a)). In this process, two different squeezed θ states are combined using a beamsplitter and photon subtraction is heralded by the detection of a single photon in one of the output channels. For optimized parameters, this process yields a cat state in the other output channel. We note that this process produces a squeezed cat state which can be unsqueezed if necessary. The parameters for this setup are: the squeezing strengths r_1, r_2 , the angles for the input states θ_1, θ_2 , the beamsplitter transmissivity represented by the angle γ and the unsqueezing strength on the output state. We optimized these parameters to yield a large success probability and fidelity, defined as $F = |\langle \text{cat}_{\alpha,-} | \text{out} \rangle|^2$, against a target cat state of size $|\alpha|^2 \in [2, 6]$. The infidelities and success probabilities are presented in Fig. 2(a).

The performance of the θ states can be interpreted by the stellar ranks of the output states. In general, the output state continuous variable wavefunction is $\psi_{\text{out}}(x) \propto (b_1 x + b_3 x^3 + b_5 x^5) e^{-cx^2}$ (see Supplemental Material (SM) for the fidelity, success probability and the stellar rank), and the stellar rank is five. In the cases when the squeezing are equal in magnitude but opposite signs, or one of the input state is in vacuum, $b_5 = 0$ and the stellar rank is three. When both conditions are simultaneously satisfied, $b_3 = b_5 = 0$ and the stellar rank is one. Note that, if both inputs are vacuum ($\theta_{1,2} = 0$), but under different squeezing strengths, $b_3 = b_5 = 0$, and our setup reduces to the generalized photon subtraction in Ref. [26] and the stellar rank is one. At first sight, it appears that using the θ state offers no advantage over using two-photon inputs as they have the same stellar rank. However, when the input states are fixed to two-photon Fock states, there is less flexibility for tuning the output wavefunction for higher success probabilities compared to the θ states. In Fig. 2(a), we compare the performance of using the θ states to the two-photon Fock states as inputs. When restricting the success probability to $P_{\text{suc}} \geq 0.25$, the two-photon Fock states can only prepare poor quality cat states. This calculation was performed using the analytic expressions for the fidelity and success probability (see SM). On the other hand, the fidelity of using the θ states is $F \geq 0.999$ for cat state of size $|\alpha|^2 \leq 3.14$, and $F \geq 0.99$ for $|\alpha|^2 \leq 5.40$. The success probability ranges from 0.529 to 0.427 which is almost twice as large as using the squeezed two-photon input states. We note that, for the same parameters, detecting two photons also produces a high-fidelity even-cat state, $|\text{cat}_{\alpha,+}\rangle$ (see SM).

In state-of-the-art experimental setups, the main source of imperfection is loss and imperfect photon de-

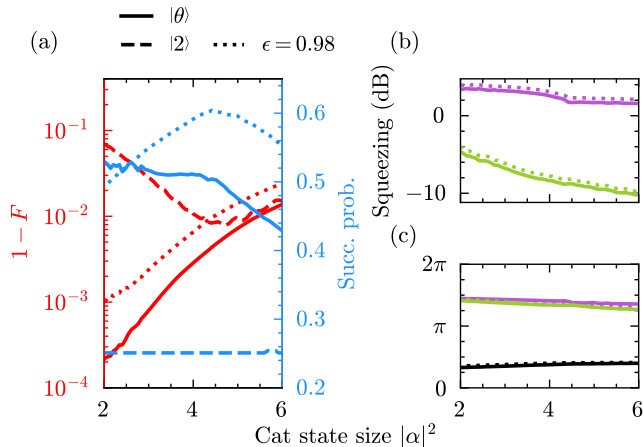


FIG. 2. Performance and parameters for the linear photon subtraction protocol. In (a), the optimized infidelity (red) and the success probability (blue) for generating cat states of size $|\alpha|^2 \in [2, 6]$ using the squeezed θ states (solid) and squeezed two-photon states (dashed) as inputs. In all panels, we include the re-optimized results and parameters of the θ states with detector efficiency of $\epsilon = 0.98$ (dotted). In (b) the squeezing strengths r_1 (purple), r_2 (green), note signs of the squeezing strengths correspond to squeezing in perpendicular directions. In (c), the angles θ_1 (purple), θ_2 (green) and the beamsplitter parameter γ (black).

tection. We model this by inserting a linear loss element prior to the photon detector and calculate using a discrete variable approach (see SM). The success probability and infidelity after re-optimizing the parameters with the presence of loss are shown in Fig. 2(a-c). The protocol performs remarkably well with 2% loss, with infidelity of $\leq 1\%$ for cat states with $|\alpha|^2 \leq 4$. We note that this is a significant loss tolerance compared to other protocols [14]. The robustness to loss is due to the protocol being heralded by the detection of only a single photon.

Nonlinear photon subtraction.—Although our linear optics photon subtraction protocol has a high fidelity and success probability, it uses two squeezed θ states as inputs. We now consider a nonlinear photon subtraction protocol of a single squeezed θ state using a TLS chirally coupled to a waveguide. This type of photon subtraction protocol was recently proposed using squeezed vacuum inputs [36]. We model the TLS-waveguide system under the Born-Markov and the rotating-wave approximations and renormalize to the resonance frequency of the TLS. The Hamiltonian for this system is ($\hbar = v_g = 1$)

$$\hat{H} = -i \int_{\mathbb{R}} dx \hat{a}^\dagger(x) \partial_x \hat{a}(x) + \sqrt{\Gamma} [\hat{a}^\dagger(0) \hat{\sigma}_- + \hat{\sigma}_+ \hat{a}(0)], \quad (2)$$

where $\hat{a}^\dagger(x)$ is the photon creation operator at position x , $\hat{\sigma}_\pm$ are the Pauli operators of the TLS and Γ is the coupling strength [37, 38]. Analytic expressions for the

scattering problem in the many-photon limit are typically not tractable [38, 39]. To model the multi-mode dynamics of the photon field, we adapt the discretized input-output theory in the language of matrix product states (MPS) [40–42]. In the narrow discretization limit, the solution to the quantum stochastic Schrödinger equation is well approximated by a product of the first-order-trotter-decomposed time evolution unitary operators. Further details of the MPS implementation are given in the SM.

In the nonlinear photon-subtraction protocol, the TLS scatters an input wave packet into a product state composed of an output state of interest and a single-photon state in an orthogonal temporal mode, i.e., $|\text{in}\rangle \rightarrow |\text{out}\rangle |1\rangle$. For an n -photon Fock state this is almost deterministic [36, 38, 43]. However, it was shown that photon subtraction from squeezed vacuum was not deterministic [36]. This is because the squeezed vacuum pulses with a temporally narrow width required for ideal photon subtraction cannot deterministically scatter photons into an orthogonal mode. Our nonlinear single-photon subtraction protocol is shown in Fig. 1(b). A single-mode resource state $|r, \theta_{\max}\rangle$ scatters into a multi-mode state, under the appropriate wave packet width and squeezing strength, a cat state in the dominant mode is heralded by detecting a photon from the non-dominant modes. For the best success probability we consider input states with the largest photon number. That is, we fix $\theta_{\max}(r) = \pi - \arctan(t_r/\sqrt{2})$, such that under squeezing, the mean photon number $\langle \hat{n} \rangle = c_r(\sqrt{2/(t_r^2 + 2)} + 3/2) + s_r t_r / \sqrt{2(t_r^2 + 2)} - 1/2$ of the resource state is maximized; where $c_r = \cosh(2r)$, $s_r = \sinh(2r)$ and $t_r = \tanh(2r)$. We emphasize that this does not occur at $\theta = \pi$, highlighting the importance of generating θ states. Moreover, we numerically recover θ_{\max} when θ is included in one of the parameters in the optimization process (see SM). Since the total number of excitations in the waveguide is conserved in the scattering process, $\theta_{\max}(r)$ also maximizes the mean photon number in the dominant mode, leading to the largest generated cat state.

To implement the nonlinear photon subtraction we launch the input state $|r, \theta_{\max}\rangle$ into a Gaussian wave packet and compute the scattering process using the MPS formalism (see SM). We find the dominant mode of the output state by computing and diagonalizing the first-order coherence $G^{(1)}(t, t') = \langle \hat{a}^\dagger(t) \hat{a}(t') \rangle = \sum_i \bar{n}_i v_i^*(t) v_i(t')$, where $v_i(t)$ are a set of orthonormal modes and \bar{n}_i are the corresponding mean photon numbers in each mode [44]. This allows us to extract the dominant mode out of the waveguide with a virtual cavity [44]. In an experiment this is performed using a quantum pulse gate (QPG) [45]. Furthermore, we project the waveguide onto the single-photon sector by tracing over all possible single-photon detection events. The protocol thus assumes photon number resolving detection but does not require any timing resolution. Lastly,

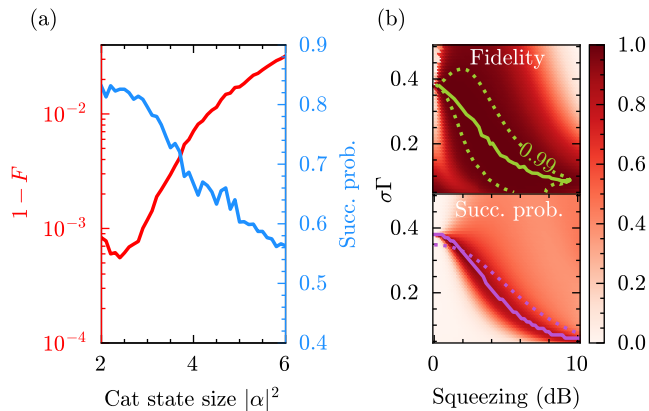


FIG. 3. The fidelity and the success probability for the nonlinear photon subtraction scheme. In (a), the best infidelity (red) and success probability (blue) for generating cat state of size $|\alpha|^2$. In (b), the fidelity (top) and the success probability (bottom) across various input width $\sigma\Gamma$ and squeezing strength r . The dashed green contour encloses regions with fidelity $F > 0.99$ and the green (purple) solid line highlights the best fidelity (success probability). The dotted purple line shows the values for inverting the atom using a π -pulse model.

the state in the virtual cavity is the output state of the protocol. In essence, the input state transforms like $|r, \theta_{\max}(r)\rangle \rightarrow |\text{out}\rangle|1\rangle$, where $|\text{out}\rangle$ contains the most number of photon in the waveguide. Ideally, the resource state scatters into a two-mode product state, where the second most dominant mode contains a single-photon, thus making the protocol deterministic. However, with the presence of vacuum and higher photon-number subtraction events, ultimately, the protocol becomes nearly deterministic.

We numerically sample across various wave packet widths and squeezing strengths and demonstrate regions of high success probabilities ($P_{\text{succ}} > 0.8$) of single-photon subtraction, see Fig. 3(b). To achieve maximum fidelity against a pure target state, one must also maximize the purity of the prepared state. The scattered photon field is approximately occupied by two modes (a dominant mode captured by the virtual cavity and an ancillary mode in the field), consequently, tracing over all single-photon detection events in the field maintains high purity of the output state (see SM). In Fig. 3(b), we show the fidelity of the virtual cavity (dominant mode), defined as $F = \langle \text{cat}_{\alpha,-} | \hat{\rho}_{\text{out}} | \text{cat}_{\alpha,-} \rangle$ against an optimally chosen sized cat state. Moreover, region of high fidelity ($F > 0.99$) is enclosed by the dashed green contour and the highest fidelity is highlighted by the green line. Remarkably, the line of the highest success probability (purple) overlaps with the line of the highest fidelity for squeezing strength up to 7 dB corresponding to the generated cat state of size up to $|\alpha|^2 \approx 3$. To generate larger cat states, the success probability is sacrificed to achieve

optimal fidelity. A simple π -pulse model, which models the excited state population of the TLS as though it is driven by a coherent field, can be used to determine the values for which high success probability occurs. By finding squeezing and σ values such that $2 \int dt \sqrt{\Gamma} \langle \hat{n}(t) \rangle = \pi$, the regions of high success probability are near where the TLS is inverted by the input field. In Fig. 3(a), we showcase the best infidelity and the corresponding success probability for generating cat states of size $|\alpha|^2 \in [2, 6]$. Again, the characteristic trade-off between fidelity and success probability is present, nonetheless our protocol managed $F \geq 0.99$ and $P_{\text{succ}} \geq 0.664$ for cat state size $|\alpha|^2 \leq 4.3$. For larger cat states the fidelity is ultimately limited by the stellar rank of the input state which, after squeezing and photon subtraction, which only allows high-fidelity approximations for cats states with $|\alpha|^2 \lesssim 4$. In contrast to the linear protocol, the nonlinear protocol has higher success probabilities using a single θ state.

Preparation of the θ state.—We first consider a linear optics implementation that probabilistically heralds the generation of a θ state using single-photon states as inputs. Consider a beamsplitter setup similar to the one in Fig. 1(a), but with states $|\phi_i\rangle = \cos(\phi_i/2)|0\rangle + \sin(\phi_i/2)|1\rangle$ input in the top $i=1$ and bottom $i=2$. Such superposition states can easily be generated from any TLS photon source by preparing it in a superposition of excited and ground states. After these two states mix at a 50:50 beamsplitter the generation of a $|\theta\rangle$ state is heralded by the absence of photon clicks in the output detector. With state-of-the-art circuits, beamsplitters, and detectors; photon loss—which spoils the fidelity—can be made very small [46]. For the correct state to be produced we require $\phi_2 = -\phi_1$, which produces $|\text{out}\rangle = [\cos^2(\phi_1/2)|0\rangle - \sin^2(\phi_1/2)|2\rangle]/\sqrt{2}]/\sqrt{P_{\text{succ}}}$ with a success probability of $P_{\text{succ}}(\phi_1) = \cos^4(\phi_1/2) + \sin^4(\phi_1/2)/2$, which has $1/3 \leq P_{\text{succ}} \leq 1$ depending on the desired angle of the θ state. To obtain a desired angle θ we find the correct value of ϕ_1 by solving the equation $\cos(\theta/2) = \cos^2(\phi_1/2)/\sqrt{P_{\text{succ}}(\phi_1)}$. Finally, we note the minus sign in $|\text{out}\rangle$, which is different to the θ state definition. This can be compensated for by adding a $\pi/2$ phase element to the optical path when values of $0 \leq \theta \leq \pi$ are required.

We now consider deterministic generation using two three-level atoms coupled to an optical cavity with equivalent couplings. The three-level atoms each have a ground state $|g\rangle$ optically coupled to an excited state $|e\rangle$, and a shelving state $|s\rangle$. We can use this system to generate $|\theta\rangle$ by first preparing the two atoms in the state $(\cos(\theta/2)|g\rangle + \sin(\theta/2)|s\rangle)|g\rangle$. We then perform a controlled-NOT gate within the s, g subspace where $|g\rangle$ ($|s\rangle$) encodes the zero (one) state. The first atom represented by the first ket acts as the control qubit and the second the target. Here, atomic systems with Rydberg transitions are ideal for implementing such a gate with very high fidelity [47]. This prepares the state

$(\cos(\theta/2)|gg\rangle + \sin(\theta/2)|ss\rangle)$. By performing an optical π pulse on the s - e transition, the population is moved coherently from s to e , and the atoms then decay along the e - g transition. The atom-photon system is left in the state $|\bar{\theta}\rangle|gg\rangle = (\cos(\theta/2)|0\rangle + \sin(\theta/2)|\bar{2}\rangle)|gg\rangle$. We note that the two-photon state $|\bar{2}\rangle$ is not a Fock state, but rather a superradiant state (see SM) with two-photon wavefunction (for $x_1 \geq x_2$),

$$\psi(x_1, x_2) = \sqrt{2}\Gamma\theta(-x_1)\theta(-x_2)e^{\Gamma x_2/2}, \quad (3)$$

where $\theta(x)$ is Heaviside's step function. Since our protocols require single-moded states, we calculate the fidelity of the state $|\bar{\theta}\rangle$ by finding the dominant mode of $\psi(x_1, x_2)$ and computing $F = |\langle\theta|\bar{\theta}\rangle|^2$. We find that the infidelity is $1 - F \sim 2\sin^2(\theta/2)0.046$ with $0.046 = 1 - \langle 2|\bar{2}\rangle$ corresponding to a minimal fidelity of $F_{\min} \sim 0.91$ (see SM). We can also add the influence of imperfect coupling. This can be done by considering a coupling efficiency β to the collection channel. With imperfect coupling the minimal fidelity is $F_{\min} \sim 1 - 2(1 - 0.954\beta)$ (see SM).

To improve the fidelity of the deterministically generated θ state we propose using process of *modal purification*. The two-photon wavefunction $\psi_2(x_1, x_2)$ can be written as a sum of a product of separable functions $\phi_i(x)$ and therefore as a sum of two-photon Fock states occupying different modes. This combination can be purified into a single Fock state by passing it through a QPG similar to that shown in Fig. 1(b). The QPG absorbs the dominant two-photon Fock state and the remainder of the state passes to a detector. The absence of a click heralds a successful purification process, while any click on the detector indicates failure and the state is discarded. The purification process therefore converts the infidelity of the state into heralded errors. In principle, this produces an ideal state. Experimentally, QPGs have already been developed with fidelity of 96% when operating with single photons [45].

Conclusion.—We have proposed using squeezed superpositions of zero and two-photon states for generating cat states. Our linear and nonlinear protocols both have high success probabilities and can generate cat states with $|\alpha|^2 \leq 5$ with near-unity fidelity. We anticipate that cat states generated using our protocols can be used as building blocks for generating larger non-Gaussian states via breeding protocols [2, 15]. Our protocols have the potential to be integrated into state-generation protocols for error-corrected quantum computing with GKP states [3, 48].

Acknowledgments.—S.M. acknowledges support from the Australian Research Council (ARC) via the Future Fellowship, ‘Emergent many-body phenomena in engineered quantum optical systems’, project no. FT200100844. H.L. acknowledges the financial support from Sydney Quantum Academy, Sydney, NSW, Australia.

* haoyuan.luo@sydney.edu.au

† sahand.mahmoodian@sydney.edu.au

- [1] D. Gottesman, A. Kitaev, and J. Preskill, Encoding a qubit in an oscillator, *Phys. Rev. A* **64**, 012310 (2001).
- [2] D. J. Weigand and B. M. Terhal, Generating grid states from schrödinger-cat states without postselection, *Phys. Rev. A* **97**, 022341 (2018).
- [3] S. Konno, W. Asavanant, F. Hanamura, H. Nagayoshi, K. Fukui, A. Sakaguchi, R. Ide, F. China, M. Yabuno, S. Miki, H. Terai, K. Takase, M. Endo, P. Marek, R. Filip, P. van Loock, and A. Furusawa, Logical states for fault-tolerant quantum computation with propagating light, *Science* **383**, 289 (2024).
- [4] T. C. Ralph, A. Gilchrist, G. J. Milburn, W. J. Munro, and S. Glancy, Quantum computation with optical coherent states, *Phys. Rev. A* **68**, 042319 (2003).
- [5] M. Bergmann and P. van Loock, Quantum error correction against photon loss using multicomponent cat states, *Phys. Rev. A* **94**, 042332 (2016).
- [6] L. Li, C.-L. Zou, V. V. Albert, S. Muralidharan, S. M. Girvin, and L. Jiang, Cat codes with optimal decoherence suppression for a lossy bosonic channel, *Phys. Rev. Lett.* **119**, 030502 (2017).
- [7] Q. Xu, G. Zheng, Y.-X. Wang, P. Zoller, A. A. Clerk, and L. Jiang, Autonomous quantum error correction and fault-tolerant quantum computation with squeezed cat qubits, *npj Quantum Information* **9**, 78 (2023).
- [8] D. S. Schlegel, F. Minganti, and V. Savona, Quantum error correction using squeezed schrödinger cat states, *Phys. Rev. A* **106**, 022431 (2022).
- [9] H. Le Jeannic, A. Cavaillès, K. Huang, R. Filip, and J. Laurat, Slowing quantum decoherence by squeezing in phase space, *Phys. Rev. Lett.* **120**, 073603 (2018).
- [10] A. L. Grimsmo, J. Combes, and B. Q. Baragiola, Quantum computing with rotation-symmetric bosonic codes, *Phys. Rev. X* **10**, 011058 (2020).
- [11] C. Chamberland, K. Noh, P. Arrangoiz-Arriola, E. T. Campbell, C. T. Hann, J. Iverson, H. Putterman, T. C. Bohdanowicz, S. T. Flammia, A. Keller, G. Refael, J. Preskill, L. Jiang, A. H. Safavi-Naeini, O. Painter, and F. G. Brandão, Building a fault-tolerant quantum computer using concatenated cat codes, *PRX Quantum* **3**, 010329 (2022).
- [12] L. Gravina, F. Minganti, and V. Savona, Critical schrödinger cat qubit, *PRX Quantum* **4**, 020337 (2023).
- [13] J. Lee, N. Kang, S.-H. Lee, H. Jeong, L. Jiang, and S.-W. Lee, Fault-tolerant quantum computation by hybrid qubits with bosonic cat code and single photons, *PRX Quantum* **5**, 030322 (2024).
- [14] M. S. Winnel, J. J. Guanzon, D. Singh, and T. C. Ralph, Deterministic preparation of optical squeezed cat and gottesman-kitaev-preskill states, *Phys. Rev. Lett.* **132**, 230602 (2024).
- [15] D. V. Sychev, A. E. Ulanov, A. A. Pushkina, M. W. Richards, I. A. Fedorov, and A. I. Lvovsky, Enlargement of optical schrödinger's cat states, *Nature Photonics* **11**, 379 (2017).
- [16] A. Ourjoumtsev, H. Jeong, R. Tualle-Brouri, and P. Grangier, Generation of optical ‘schrödinger cats’ from photon number states, *Nature* **448**, 784 (2007).
- [17] A. P. Lund, H. Jeong, T. C. Ralph, and M. S. Kim,

- Conditional production of superpositions of coherent states with inefficient photon detection, *Phys. Rev. A* **70**, 020101 (2004).
- [18] A. Laghaout, J. S. Neergaard-Nielsen, I. Rigas, C. Kragh, A. Tipsmark, and U. L. Andersen, Amplification of realistic schrödinger-cat-state-like states by homodyne heralding, *Phys. Rev. A* **87**, 043826 (2013).
- [19] C. Weedbrook, S. Pirandola, R. García-Patrón, N. J. Cerf, T. C. Ralph, J. H. Shapiro, and S. Lloyd, Gaussian quantum information, *Rev. Mod. Phys.* **84**, 621 (2012).
- [20] U. Chabaud, D. Markham, and F. Grosshans, Stellar representation of non-gaussian quantum states, *Phys. Rev. Lett.* **124**, 063605 (2020).
- [21] M. Dakna, T. Anhut, T. Opatrny, L. Knöll, and D.-G. Welsch, Generating schrödinger-cat-like states by means of conditional measurements on a beam splitter, *Phys. Rev. A* **55**, 3184 (1997).
- [22] A. Ourjoumtsev, R. Tualle-Brouri, J. Laurat, and P. Grangier, Generating optical schrödinger kittens for quantum information processing, *Science* **312**, 83 (2006).
- [23] A. E. B. Nielsen and K. Mølmer, Transforming squeezed light into a large-amplitude coherent-state superposition, *Phys. Rev. A* **76**, 043840 (2007).
- [24] H. Takahashi, K. Wakui, S. Suzuki, M. Takeoka, K. Hayasaka, A. Furusawa, and M. Sasaki, Generation of large-amplitude coherent-state superposition via ancilla-assisted photon subtraction, *Phys. Rev. Lett.* **101**, 233605 (2008).
- [25] G. S. Thekkadath, B. A. Bell, I. A. Walmsley, and A. I. Lvovsky, Engineering Schrödinger cat states with a photonic even-parity detector, *Quantum* **4**, 239 (2020).
- [26] K. Takase, J.-i. Yoshikawa, W. Asavanant, M. Endo, and A. Furusawa, Generation of optical schrödinger cat states by generalized photon subtraction, *Phys. Rev. A* **103**, 013710 (2021).
- [27] J. S. Neergaard-Nielsen, B. M. Nielsen, C. Hettich, K. Mølmer, and E. S. Polzik, Generation of a superposition of odd photon number states for quantum information networks, *Phys. Rev. Lett.* **97**, 083604 (2006).
- [28] A. Ourjoumtsev, A. Dantan, R. Tualle-Brouri, and P. Grangier, Increasing entanglement between gaussian states by coherent photon subtraction, *Phys. Rev. Lett.* **98**, 030502 (2007).
- [29] M. Eaton, C. González-Arciniegas, R. N. Alexander, N. C. Menicucci, and O. Pfister, Measurement-based generation and preservation of cat and grid states within a continuous-variable cluster state, *Quantum* **6**, 769 (2022).
- [30] N. Tomm, A. Javadi, N. O. Antoniadis, D. Najer, M. C. Löbl, A. R. Korsch, R. Schott, S. R. Valentin, A. D. Wieck, A. Ludwig, and R. J. Warburton, A bright and fast source of coherent single photons, *Nature Nanotechnology* **16**, 399 (2021).
- [31] P. Thomas, L. Ruscio, O. Morin, and G. Rempe, Efficient generation of entangled multiphoton graph states from a single atom, *Nature* **608**, 677 (2022).
- [32] M. Takeoka, H. Takahashi, and M. Sasaki, Large-amplitude coherent-state superposition generated by a time-separated two-photon subtraction from a continuous-wave squeezed vacuum, *Phys. Rev. A* **77**, 062315 (2008).
- [33] P. Marek, H. Jeong, and M. S. Kim, Generating “squeezed” superpositions of coherent states using photon addition and subtraction, *Phys. Rev. A* **78**, 063811 (2008).
- [34] D. Menzies and R. Filip, Gaussian-optimized preparation of non-gaussian pure states, *Phys. Rev. A* **79**, 012313 (2009).
- [35] I. Tzitrin, J. E. Bourassa, N. C. Menicucci, and K. K. Sabapathy, Progress towards practical qubit computation using approximate Gottesman-Kitaev-Preskill codes, *Phys. Rev. A* **101**, 032315 (2020).
- [36] M. M. Lund, F. Yang, V. R. Christiansen, D. Kornovan, and K. Mølmer, Subtraction and addition of propagating photons by two-level emitters, *Phys. Rev. Lett.* **133**, 103601 (2024).
- [37] P. Lodahl, S. Mahmoodian, S. Stobbe, A. Rauschenbeutel, P. Schneeweiss, J. Volz, H. Pichler, and P. Zoller, Chiral quantum optics, *Nature* **541**, 473 (2017).
- [38] S. Mahmoodian, G. Calajó, D. E. Chang, K. Hammerer, and A. S. Sørensen, Dynamics of many-body photon bound states in chiral waveguide qed, *Phys. Rev. X* **10**, 031011 (2020).
- [39] B. Q. Baragiola, R. L. Cook, A. M. Brańczyk, and J. Combes, n -photon wave packets interacting with an arbitrary quantum system, *Phys. Rev. A* **86**, 013811 (2012).
- [40] C. Schön, E. Solano, F. Verstraete, J. I. Cirac, and M. M. Wolf, Sequential generation of entangled multi-qubit states, *Phys. Rev. Lett.* **95**, 110503 (2005).
- [41] C. Schön, K. Hammerer, M. M. Wolf, J. I. Cirac, and E. Solano, Sequential generation of matrix-product states in cavity qed, *Phys. Rev. A* **75**, 032311 (2007).
- [42] H. Pichler and P. Zoller, Photonic circuits with time delays and quantum feedback, *Phys. Rev. Lett.* **116**, 093601 (2016).
- [43] M. M. Lund, F. Yang, and K. Mølmer, Perfect splitting of a two-photon pulse, *Phys. Rev. A* **107**, 023715 (2023).
- [44] A. H. Kiilerich and K. Mølmer, Input-output theory with quantum pulses, *Phys. Rev. Lett.* **123**, 123604 (2019).
- [45] L. Serino, J. Gil-Lopez, M. Stefszky, R. Ricken, C. Eigner, B. Brecht, and C. Silberhorn, Realization of a multi-output quantum pulse gate for decoding high-dimensional temporal modes of single-photon states, *PRX Quantum* **4**, 020306 (2023).
- [46] K. Alexander, A. Bahgat, A. Benyamini, D. Black, D. Bonneau, S. Burgos, B. Burrige, G. Campbell, G. Catalano, A. Ceballos, C.-M. Chang, C. Chung, F. Danesh, T. Dauer, M. Davis, E. Dudley, P. Er-Xuan, J. Fargas, A. Farsi, C. Fenrich, J. Frazer, M. Fukami, Y. Ganesan, G. Gibson, M. Gimeno-Segovia, S. Goeldi, P. Goley, R. Haislmaier, S. Halimi, P. Hansen, S. Hardy, J. Horng, M. House, H. Hu, M. Jadidi, H. Johansson, T. Jones, V. Kamineni, N. Kelez, R. Koustuban, G. Kovall, P. Krogen, N. Kumar, Y. Liang, N. Li-Causi, D. Llewellyn, K. Lokovic, M. Lovelady, V. Manfrinato, A. Melnichuk, M. Souza, G. Mendoza, B. Moores, S. Mukherjee, J. Munns, F.-X. Musalem, F. Najafi, J. L. O’Brien, J. E. Ortmann, S. Pai, B. Park, H.-T. Peng, N. Penthorn, B. Peterson, M. Poush, G. J. Pryde, T. Ramprasad, G. Ray, A. Rodriguez, B. Roxworthy, T. Rudolph, D. J. Saunders, P. Shadbolt, D. Shah, H. Shin, J. Smith, B. Sohn, Y.-I. Sohn, G. Son, C. Sparrow, M. Staffaroni, C. Stavarakas, V. Sukumaran, D. Tamborini, M. G. Thompson, K. Tran, M. Triplet, M. Tung, A. Vert, M. D. Vidrighin, I. Vorobeichik, P. Weigel, M. Wingert, J. Wooding, and X. Zhou, A manufacturable platform for photonic quantum computing, arXiv preprint arXiv:2404.17570 (2024).
- [47] H. Levine, A. Keesling, G. Semeghini, A. Omran, T. T.

- Wang, S. Ebadi, H. Bernien, M. Greiner, V. Vuletić, H. Pichler, and M. D. Lukin, Parallel implementation of high-fidelity multiqubit gates with neutral atoms, *Phys. Rev. Lett.* **123**, 170503 (2019).
- [48] J. E. Bourassa, R. N. Alexander, M. Vasmer, A. Patil, I. Tzitrin, T. Matsuura, D. Su, B. Q. Baragiola, S. Guha, G. Dauphinais, K. K. Sabapathy, N. C. Menicucci, and I. Dhand, Blueprint for a Scalable Photonic Fault-Tolerant Quantum Computer, *Quantum* **5**, 392 (2021).

Supplemental material for “Efficient optical cat state generation using squeezed few-photon superposition states”

Haoyuan Luo^{1,2} and Sahand Mahmoodian^{1,3}

¹*Centre for Engineered Quantum Systems, School of Physics,
The University of Sydney, NSW 2006, Australia*

²*Sydney Quantum Academy, Sydney, NSW, Australia*

³*Institute for Photonics and Optical Sciences (IPOS),
School of Physics, The University of Sydney, NSW 2006, Australia*

The supplemental material provides technical details for the main text. In Sec. I, we compare the mean photon number of the θ states and few-photon Fock states. Sec. II provides further details and calculations of the linear photon subtraction protocol. Further details on the dynamics of the photon field and time evolution in the MPS formalism for the nonlinear photon subtraction protocol are given in Sec. III. Finally, in Sec. IV, we provide details on the deterministic generation of the θ states.

I. SQUEEZED $|\theta\rangle$ STATE AND THE MEAN PHOTON NUMBER

In this section, we calculate the mean photon number and $\theta_{\max}(r)$ showcasing the flexibility of the θ states under squeezing compared to Fock states. Starting with the squeezing operator identities,

$$\hat{S}^\dagger(r)\hat{a}\hat{S}(r) = \hat{a} \cosh r + \hat{a}^\dagger \sinh r, \quad \hat{S}^\dagger(r)\hat{a}^\dagger\hat{S}(r) = \hat{a}^\dagger \cosh r + \hat{a} \sinh r. \quad (\text{S1})$$

The mean photon number is,

$$\langle \theta | \hat{S}^\dagger(r)\hat{n}\hat{S}(r) | \theta \rangle = \cosh(2r) \left(\frac{3}{2} - \cos(\theta) \right) + \frac{\sinh(2r)}{\sqrt{2}} \sin(\theta) - \frac{1}{2} \quad (\text{S2})$$

The maximum and minimum are

$$\theta_{\max}(r) = \pi - \arctan\left(\frac{\tanh(2r)}{\sqrt{2}}\right), \quad \theta_{\min}(r) = 2\pi - \arctan\left(\frac{\tanh(2r)}{\sqrt{2}}\right) \quad (\text{S3})$$

for $\theta \in [0, 2\pi)$. The mean photon number with $\theta_{\max(+), \min(-)}(r)$ are

$$\cosh(2r) \left(\pm \sqrt{\frac{2}{\tanh^2(2r) + 2}} + \frac{3}{2} \right) \pm \frac{\sinh(2r) \tanh(2r)}{\sqrt{2(\tanh^2(2r) + 2)}} - \frac{1}{2}. \quad (\text{S4})$$

In Fig. S1, we compare the mean photon number of the squeezed θ states to that of the vacuum, single and two-photon states. Choosing $\theta = \theta_{\max}(r)$, the squeezed θ states have larger mean photon numbers than the squeezed two-photon states, while choosing $\theta = \theta_{\min}(r)$ gives a smaller average photon number than squeezed vacuum. This highlights the flexibility of the θ states under squeezing.

II. LINEAR PHOTON SUBTRACTION

Here we provide the details of the linear photon subtraction protocol using a beamsplitter. Particularly, we calculate the single-photon subtracted output state wavefunction and the stellar rank using continuous variables. The many-photon subtracted output states while considering detector inefficiencies are calculated using discrete variables. Additionally, we demonstrate the performance of the θ states by comparing to that of the single and two-photon states inputs (Fig. S2). Lastly, we consider the output state after many-photon subtraction events by showing their Wigner functions (Fig. S3), and surprisingly, the two-photon subtracted state is also a high quality even-cat state (Fig. S4).

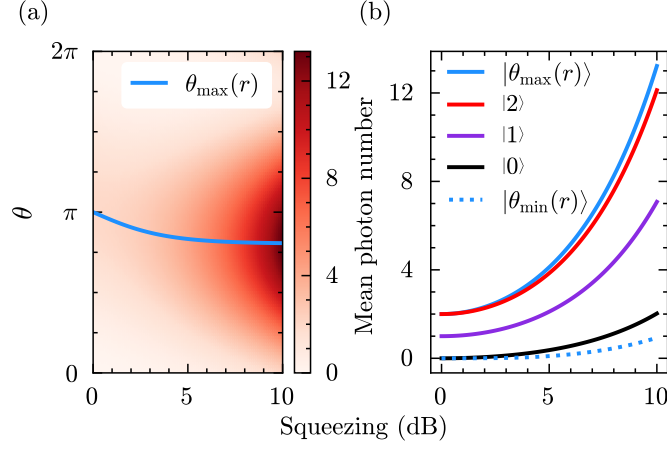


FIG. S1. Mean photon number of few-photon states under squeezing. (a) Mean photon number of the $|r, \theta\rangle$ state, the blue line highlights $\theta_{\max}(r)$. (b) Mean photon number of $\theta_{\max, \min}(r)$ (blue, dotted blue), vacuum (black), single (purple) and two-photon (red) states.

A. Continuous variable calculation

To calculate the exact analytic continuous variable position wavefunction of the single-photon subtracted output state. First, we conveniently transform the beamsplitter unitary, parameterized by γ , to real coefficients by transforming the second mode operators $i\hat{a}_2 \rightarrow \hat{a}_2$ and $i\hat{b}_2 \rightarrow \hat{b}_2$, effectively, the input and output modes are now related by

$$\begin{pmatrix} \hat{a}_1 \\ \hat{a}_2 \end{pmatrix} = \begin{pmatrix} \cos(\gamma) & -\sin(\gamma) \\ \sin(\gamma) & \cos(\gamma) \end{pmatrix} \begin{pmatrix} \hat{b}_1 \\ \hat{b}_2 \end{pmatrix}. \quad (\text{S5})$$

Since the squeezing operator and the operator to create a θ state from vacuum consist of even powers of the annihilation and creation operators, effectively, the squeezing strength and angle are transformed into $r_2 \rightarrow -r_2$ and $\theta_2 \rightarrow -\theta_2$. We now define the position and momentum operators of the output modes $\hat{x}_j = 1/\sqrt{2}(\hat{b}_j + \hat{b}_j^\dagger)$ and $\hat{p}_j = i/\sqrt{2}(\hat{b}_j^\dagger - \hat{b}_j)$, where $j = 1, 2$ denote the output modes. Under the action of the beamsplitter, the output position variables (x_1, x_2) are related to the input position variables (x'_1, x'_2) by

$$\begin{pmatrix} x'_1 \\ x'_2 \end{pmatrix} = \begin{pmatrix} \cos(\gamma) & \sin(\gamma) \\ -\sin(\gamma) & \cos(\gamma) \end{pmatrix} \begin{pmatrix} x_1 \\ x_2 \end{pmatrix}. \quad (\text{S6})$$

The wavefunction for the squeezed vacuum state is [1]

$$\psi(x) = \pi^{-1/4} s^{-1/2} e^{-x^2/2s^2}, \quad (\text{S7})$$

where $s = e^r$. Hence, the wavefunction for a squeezed θ state is

$$\Psi_i(x) = \left[\cos\left(\frac{\theta_i}{2}\right) + \sin\left(\frac{\theta_i}{2}\right) \left(\frac{\sqrt{2}x^2}{s_i^2} - \frac{1}{\sqrt{2}} \right) \right] \psi(x), \quad (\text{S8})$$

where $i = 1, 2$ denote the output modes. Projecting one of output modes, parametrized by x_2 , onto the single-photon Fock state yields the unnormalized wavefunction

$$\psi_{\text{out}}(x_1) = \int_{-\infty}^{\infty} dx_2 \Psi_1(\cos \gamma x_1 + \sin \gamma x_2) \Psi_2(-\sin \gamma x_1 + \cos \gamma x_2) \psi_1(x_2), \quad (\text{S9})$$

where $\psi_1(x) = \sqrt{2}\pi^{-1/4} x e^{-x^2/2}$ is the single-photon Fock state wavefunction. Focusing on the exponential terms and completing the square yields

$$\exp\left[-(\cos \gamma x_1 + \sin \gamma x_2)^2/2s_1^2 - (-\sin \gamma x_1 + \cos \gamma x_2)^2/2s_2^2 - x_2^2/2\right] \quad (\text{S10})$$

$$= \exp[-a(x_2 + bx_1/a)^2] \exp[-cx_1^2], \quad (\text{S11})$$

where

$$a = [\sin^2(\gamma)/s_1^2 + \cos^2(\gamma)/s_2^2 + 1]/2, \quad b = (1/s_1^2 - 1/s_2^2) \sin(2\gamma)/4, \quad c = [\cos^2(\gamma)/s_1^2 + \sin^2(\gamma)/s_2^2 - 2b^2/a]/2. \quad (\text{S12})$$

This form allows us to integrate the expression using the relation

$$\int_{-\infty}^{\infty} dx x^n e^{-\alpha(x+\beta)^2} = \sum_{k=0}^{\lfloor n/2 \rfloor} \binom{n}{2k} (-\beta)^{n-2k} \sqrt{\frac{\pi}{\alpha}} \frac{(2k-1)!!}{2^k \alpha^k}, \quad (\text{S13})$$

for $\alpha > 0$ and $\beta \in \mathbb{R}$.

After the beamsplitter, the unnormalized position wavefunction, conditioned on detecting a single photon in the output mode with annihilation operator \hat{b}_2 , is

$$\psi_{\text{out}}(x_1) = \pi^{-1/4} \sqrt{\frac{2}{s_1 s_2 a}} e^{-c x_1^2} (b_1 x_1 + b_3 x_1^3 + b_5 x_1^5) \quad (\text{S14})$$

where

$$b_1 = \frac{1}{a} \left[-Ab + \frac{B-C}{2} \sin(2\gamma) - \frac{3b}{2a} (B \sin^2(\gamma) + C \cos^2(\gamma)) + \frac{3}{8a} D \sin(4\gamma) - \frac{15b}{16a^2} D \sin^2(2\gamma) \right], \quad (\text{S15})$$

$$b_3 = -\frac{b}{a} (B \cos^2(\gamma) + C \sin^2(\gamma)) + \frac{D \sin(4\gamma)}{2a} \left(\frac{3b^2}{a^2} - \frac{1}{2} \right) + \frac{b^2}{a^2} (B-C) \sin(2\gamma) - \frac{b^3}{a^3} (B \sin^2(\gamma) + C \cos^2(\gamma)) \quad (\text{S16})$$

$$- \frac{3b}{2a^2} D \left(\cos(4\gamma) + \frac{\sin^2(2\gamma)}{2} \right) - \frac{5b^3}{4a^4} D \sin^2(2\gamma), \quad (\text{S17})$$

$$b_5 = \frac{Db}{a} \left[- \left(\frac{b^4}{4a^4} + \frac{b^2}{2a^2} + \frac{1}{4} \right) \sin^2(2\gamma) + \frac{b}{2a} \left(\frac{b^2}{a^2} - 1 \right) \sin(4\gamma) - \frac{b^2}{a^2} \cos(4\gamma) \right], \quad (\text{S18})$$

and,

$$A = \left[\cos(\theta_1/2) - \sin(\theta_1/2)/\sqrt{2} \right] \left[\cos(\theta_2/2) - \sin(\theta_2/2)/\sqrt{2} \right], \quad B = \sqrt{2} s_1^{-2} \sin(\theta_1/2) \left[\cos(\theta_2/2) - \sin(\theta_2/2)/\sqrt{2} \right], \quad (\text{S19})$$

$$C = \sqrt{2} s_2^{-2} \sin(\theta_2/2) \left[\cos(\theta_1/2) - \sin(\theta_1/2)/\sqrt{2} \right], \quad D = 2 s_1^{-2} s_2^{-2} \sin(\theta_1/2) \sin(\theta_2/2). \quad (\text{S20})$$

The success probability, $P_{\text{suc}} = \int dx_1 |\psi_{\text{out}}(x_1)|^2$ is

$$P_{\text{suc}} = \frac{\sqrt{2}}{s_1 s_2 a \sqrt{c}} \left[\frac{b_1^2}{4c} + \frac{3b_1 b_3}{8c^2} + \frac{15(b_3^2 + 2b_1 b_5)}{64c^3} + \frac{105b_3 b_5}{128c^4} + \frac{945b_5^2}{1024c^5} \right]. \quad (\text{S21})$$

The wavefunction for a squeezed odd cat state, $|\text{Cat}_{\alpha,-}\rangle \propto \hat{S}(r)[\hat{D}(\alpha) - \hat{D}(-\alpha)]|0\rangle$ is [2]

$$\psi_{\text{cat}}(x) = \frac{e^{\alpha^2}}{\sqrt{N_{\text{cat}}}} \left[e^{-(x-\sqrt{2}\alpha s)^2/2s^2} - e^{-(x+\sqrt{2}\alpha s)^2/2s^2} \right], \quad (\text{S22})$$

$$N_{\text{cat}} = 2 \left(1 - e^{-2|\alpha|^2} \right) \pi^{1/2} s e^{(\alpha+\alpha^*)^2/2}. \quad (\text{S23})$$

Hence, the fidelity, $F = |\langle \text{Cat}_{\alpha,-} | \text{out} \rangle|^2$ is

$$F = \frac{16\sqrt{\pi}s^2}{N_{\text{cat}} P_{\text{suc}} s_1 s_2 a (2s^2 c + 1)} \left| e^{\alpha^2/(2s^2 c + 1)} \right|^2 \quad (\text{S24})$$

$$\left| \left(b_1 + \frac{3s^2 b_3}{2s^2 c + 1} + \frac{15s^4 b_5}{(2s^2 c + 1)^2} \right) \frac{\sqrt{2}\alpha s}{2s^2 c + 1} + \left(b_3 + \frac{10s^2 b_5}{2s^2 c + 1} \right) \left(\frac{\sqrt{2}\alpha s}{2s^2 c + 1} \right)^3 + b_5 \left(\frac{\sqrt{2}\alpha s}{2s^2 c + 1} \right)^5 \right|^2. \quad (\text{S25})$$

1. Stellar rank

The stellar rank is defined by the number of zeros of the stellar function, $F^*(\alpha) := e^{|\alpha|^{1/2}} \langle \alpha^* | \psi_{\text{out}} \rangle$ [3]. The overlap with a coherent state $\langle \alpha^* |$ can be readily calculated in the position basis. The wavefunction of a coherent state $|\alpha\rangle$ is [1]

$$\psi_\alpha(x) = \pi^{-1/4} e^{-(\alpha+\alpha^*)^2/4+\alpha^2} e^{-(x-\sqrt{2}\alpha)^2/2}. \quad (\text{S26})$$

The overlap with the output state is

$$\langle \alpha^* | \psi_{\text{out}} \rangle \propto e^{-(\alpha+\alpha^*)^2/4+\alpha^2/(2c+1)} \int_{-\infty}^{\infty} dx (b_1 x + b_3 x^3 + b_5 x^5) e^{-(2c+1)[x-\sqrt{2}\alpha/(2c+1)]^2/2}. \quad (\text{S27})$$

Notice that, for $\alpha \in \mathbb{R}$, this is exactly the form of the integral given by Eq. (S13) and the solution is an n -order polynomial of α . Moreover, for $\alpha \in \mathbb{C}$, one can analytically extend the domain of the finite order polynomial to the complex plane and find the stellar function

$$F^*(\alpha) \propto e^{|\alpha|^{1/2} - \frac{(\alpha+\alpha^*)^2}{4} + \frac{\alpha^2}{2c+1}} \left[\left(b_1 + \frac{3b_3}{2c+1} + \frac{15b_5}{(2c+1)^2} \right) \frac{\sqrt{2}\alpha}{2c+1} + \left(b_3 + \frac{10b_5}{2c+1} \right) \left(\frac{\sqrt{2}\alpha}{2c+1} \right)^3 + b_5 \left(\frac{\sqrt{2}\alpha}{2c+1} \right)^5 \right]. \quad (\text{S28})$$

This expression is very general and reduces in several limiting cases. We first see that, in general, the stellar rank is five. When the squeezing strengths are equal ($b = 0$), or one of the input state is in vacuum ($D = 0$), $b_5 = 0$ and the stellar rank is three. When both conditions are simultaneously satisfied ($b = 0, D = 0$), the coefficients are $b_5 = b_3 = 0$ and the stellar rank is one. Moreover, if both input states are vacuum and subject to equal squeezing strengths, $b_1 = 0$, and the stellar rank is zero, in other words, the output state is Gaussian. However, the probability of generating such states is also zero. Nonetheless, if both inputs are vacuum but under different squeezing strengths ($b_3 = b_5 = 0$), the stellar rank is one. When the input states are fixed to two-photon Fock states, in general, the stellar rank is still five but offers less flexibility for tuning the output wavefunction compare to the θ states.

B. Discrete variable calculation

We now present the details of our calculations for linear photon subtraction using a discrete-variable approach. This is particularly useful when considering imperfect photon detection via photon loss. To obtain an analytic expression of the many-photon subtracted output state, first we express the squeezed θ states in the number basis,

$$|r, \theta\rangle = \hat{S}(r) |\theta\rangle = \sum_{n=0}^{\infty} B_n(r, \theta) |2n\rangle, \quad (\text{S29})$$

where

$$B_n(r, \theta) = \frac{\tanh^n(r)}{\sqrt{\cosh(r)}} \frac{\sqrt{(2n)!}}{2^n n!} \left(A_0 + \frac{2n}{\tanh(r)} A_+ + (2n+1) \tanh(r) A_- + 2n A_{+-} \right). \quad (\text{S30})$$

and

$$A_0 = \cos\left(\frac{\theta}{2}\right) - \sin\left(\frac{\theta}{2}\right) \frac{\sinh(2r)}{2\sqrt{2}}, \quad A_+ = \sin\left(\frac{\theta}{2}\right) \frac{\cosh(2r) + 1}{2\sqrt{2}} \quad (\text{S31})$$

$$A_- = \sin\left(\frac{\theta}{2}\right) \frac{\cosh(2r) - 1}{2\sqrt{2}}, \quad A_{+-} = -\sin\left(\frac{\theta}{2}\right) \frac{\sinh(2r)}{\sqrt{2}}. \quad (\text{S32})$$

Now consider a beamsplitter parametrized by γ and with the input modes, denoted by their annihilation operators (\hat{a}_1, \hat{a}_2) . Under conjugation of the two-mode beamsplitter unitary $\hat{U}_{1,2}(\gamma)$ the input modes are linear transformations of the output modes (\hat{b}_1, \hat{b}_2) via

$$\hat{U}_{1,2}(\gamma) \begin{pmatrix} \hat{a}_1^\dagger \\ \hat{a}_2^\dagger \end{pmatrix} \hat{U}_{1,2}^\dagger(\gamma) = \begin{pmatrix} \cos(\gamma) & i \sin(\gamma) \\ i \sin(\gamma) & \cos(\gamma) \end{pmatrix} \begin{pmatrix} \hat{b}_1^\dagger \\ \hat{b}_2^\dagger \end{pmatrix}. \quad (\text{S33})$$

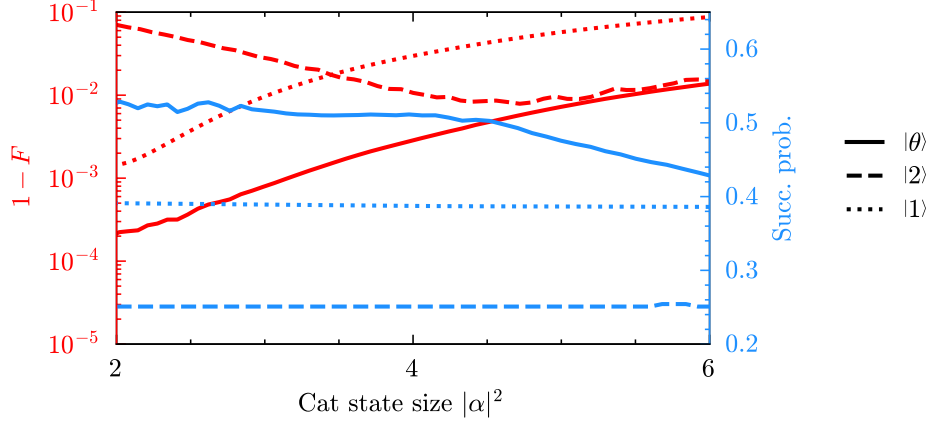


FIG. S2. The Infidelity (red) and the success probability (blue) using linear photon subtraction. When prioritizing the success probability together with the fidelity, the squeezed θ states (solid) outperforms the squeezed two-photon (dashed) and the single-photon (dotted) states as inputs, in both criteria. Note, when using the squeezed single-photons, the protocol is heralded by detecting two photons (see text).

Hence, the input states transforms like,

$$\hat{U}_{1,2}(\gamma) |r_1, \theta_1\rangle |r_2, \theta_2\rangle = \sum_{n,m=0}^{\infty} B_n(r_1, \theta_1) B_m(r_2, \theta_2) \frac{(c_\gamma \hat{b}_1^\dagger + s_\gamma \hat{b}_2^\dagger)^{2n}}{\sqrt{(2n)!}} \frac{(s_\gamma \hat{b}_1^\dagger + c_\gamma \hat{b}_2^\dagger)^{2m}}{\sqrt{(2m)!}} |0\rangle \quad (\text{S34})$$

$$= \sum_{n,m=0}^{\infty} B_n(r_1, \theta_1) B_m(r_2, \theta_2) \sum_{k=0}^{2n} \sum_{l=0}^{2m} \binom{2n}{k} \binom{2m}{l} \frac{c_\gamma^{2n-k+l} s_\gamma^{k+2m-l} \hat{b}_1^{\dagger 2n-k+2m-l} \hat{b}_2^{\dagger k+l}}{\sqrt{(2n)!(2m)!}} |0\rangle, \quad (\text{S35})$$

where $c_\gamma = \cos(\gamma)$ and $s_\gamma = i \sin(\gamma)$. Subtracting q photons in the context of a beamsplitter is realized by projecting the output mode \hat{b}_2 onto the number state $|q\rangle$ and consequently, the unnormalized output state in the mode \hat{b}_1 is

$$\langle q| \otimes \mathbf{1} \hat{U}_{1,2}(\gamma) |r_1, \theta_1\rangle |r_2, \theta_2\rangle \quad (\text{S36})$$

$$= \sum_{n=0}^{\infty} \sum_{m=\max(0, \lceil q/2 \rceil - n)}^{\infty} B_n(r_1, \theta_1) B_m(r_2, \theta_2) \sum_{k=\max(0, n - \lfloor q/2 \rfloor)}^{2n + \min(0, n - \lceil q/2 \rceil)} \binom{2n}{k} \binom{2m}{2n - k + 2m - q} \quad (\text{S37})$$

$$c_\gamma^{2k+2n-q} s_\gamma^{2(2n-k)+2m-q} \sqrt{\frac{(2n+2m-q)! q!}{(2n)!(2m)!}} |2n+2m-q\rangle. \quad (\text{S38})$$

We model inefficient detectors by placing a beamsplitter with transmission coefficient $\cos(\phi)$ before the ideal detector; the detector efficiency is $\epsilon = \cos^2(\phi)$. Again, projecting on the mode \hat{b}_2 onto the number state $|q\rangle$ and tracing over the reflected mode, denoted \hat{b}_3 , gives us the unnormalized output density matrix

$$\hat{\rho} = \sum_{p=0}^{\infty} \langle \text{out}|q\rangle |p\rangle \langle p| \langle q| \text{out}\rangle, \quad (\text{S39})$$

where $|p\rangle = \hat{b}_3^{\dagger p} / \sqrt{p!} |0\rangle$ and $|q\rangle = \hat{b}_2^{\dagger q} / \sqrt{q!} |0\rangle$. The output pure state is

$$|\text{out}\rangle = \hat{U}_{2,3}(\phi) \hat{U}_{1,2}(\gamma) |r_1, \theta_1\rangle |r_2, \theta_2\rangle |0\rangle, \quad (\text{S40})$$

where $\hat{U}_{2,3}(\phi)$ is the two-mode beamsplitter unitary acting on the modes with annihilation operators \hat{b}_2 and \hat{b}_3 . Each term in the sum can be calculated by

$$\langle p| \langle q| \text{out}\rangle = c_\phi^q s_\phi^p \sum_{n=0}^{\infty} \sum_{m=\max(0, \lceil (p+q)/2 \rceil - n)}^{\infty} B_n(r_1, \theta_1) B_m(r_2, \theta_2) \sqrt{\frac{(2n+2m-p-q)! p! q!}{(2m)!(2n)!}} |2n+2m-p-q\rangle \quad (\text{S41})$$

$$\sum_{k=\max(0, p+q-2m)}^{\min(p+q, n + \lfloor (p+q)/2 \rfloor, 2n)} \binom{2n}{k} \binom{2m}{p+q-k} c_\gamma^{2n-2k+p+q} s_\gamma^{2m+2k-p-q} \sum_{l=\max(0, k-q)}^p \binom{k}{l} \binom{p+q-k}{p-l}, \quad (\text{S42})$$

where $c_\phi = \cos(\phi)$ and $s_\phi = i \sin(\phi)$.

From Fig. S2, the θ states outperform the single and two-photon states with lower infidelities and higher success probabilities. Note that, when using the single-photon states as inputs, the protocol heralds on two-photon subtractions. This is because a trivial beamsplitter will return unit success probability and the generated cat state is then poorly approximated by a squeezed single photon state.

C. Many-photon subtracted states

We now consider the output state after many-photon subtraction events via the beamsplitter and using squeezed θ states as inputs. In Fig. S3 we plot the Wigner functions for zero to five-photon subtracted output states, under the same parameters optimized for the single-photon subtracted protocol. Remarkably, the two-photon subtracted state is a high quality even-cat state. Furthermore, in Fig. S4, we compare the infidelity and the success probability of the single-photon and two-photon subtracted output. Under the same input parameters, the two-photon subtracted output state can only produce cat states of size $|\alpha|^2 \geq 4$ but has smaller infidelities than that of the single-photon subtracted case. However, the success probabilities are much lower at ~ 0.12 .

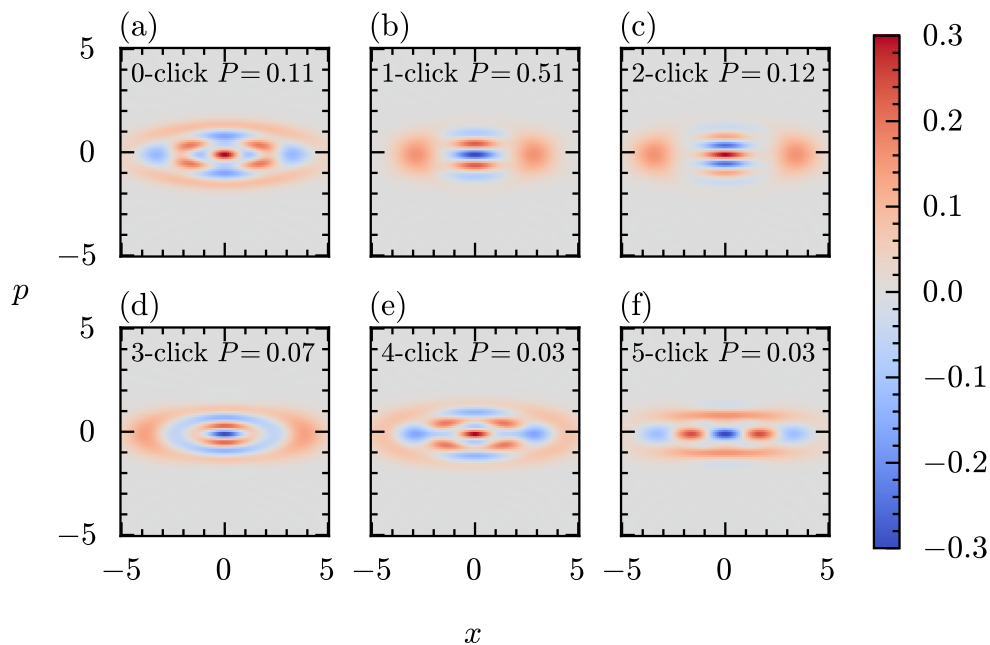


FIG. S3. The squeezed θ states are used as inputs for the beamsplitter. (a)-(f) Wigner functions of the output state, conditioned on detecting zero to five photons in one of the output modes. P is the success probability of the corresponding detection event. The parameters in all panels, $r_1, r_2, \theta_1, \theta_2, \gamma$ and the post unsqueezing strength r_{post} are optimized for (b), the single-photon subtraction output state for producing cat state of size $|\alpha|^2 = 4$. Remarkably, under the same parameters, the two-photon subtracted state in (c), is a high quality even-cat state of size $|\alpha|^2 \approx 5.9$.

III. NONLINEAR PHOTON SUBTRACTION

Here we provide more details on the nonlinear photon subtraction protocol and the photon field dynamics in the matrix product state (MPS) formalism. First, we introduce the cascaded system consisting of a virtual input cavity, the two-level system (TLS) and a virtual capture cavity. The virtual cavities are used to insert and collect a single mode into and from the one-dimensional photon bath respectively. We then write down the time-evolution unitary as a solution to the quantum stochastic Schrödinger equation. By discretizing the waveguide into small time bins, we show that the system and the photon field pure state can be written as an MPS. Time-evolution is then generated by applying local operators to the MPS. Finally, we compare the performance of the squeezed θ states to the squeezed single-photon states used as inputs.

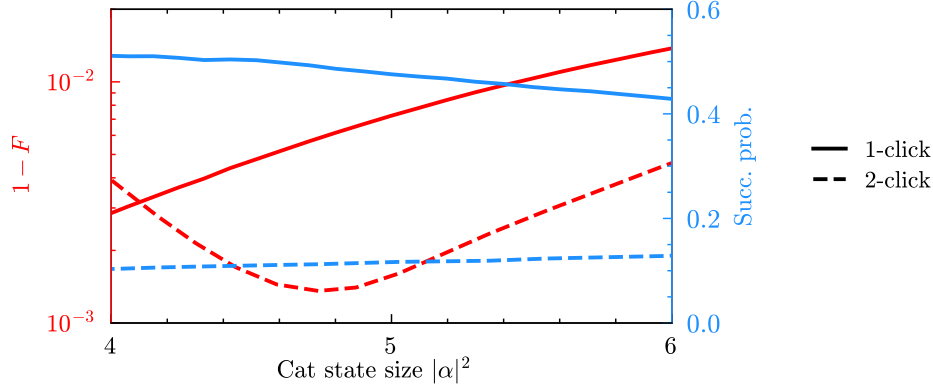


FIG. S4. Squeezed θ states are used as inputs for the beamsplitter. The infidelity (red) and the success probability (blue) for single-photon (solid) and two-photon (dashed) subtracted output states. The two-photon subtracted state uses the same input parameters as the single-photon subtracted state but the cat state size $|\alpha|^2$ and the post unsqueezing strength are further optimized for the smallest infidelities. The two-photon subtracted state can only produce cat state size of $|\alpha|^2 \geq 4$.

We consider a one dimensional waveguide with a TLS chirally coupled to a right-propagating photon field. We include two virtual cavities to model the release and capture of photons in specific temporal modes. Together, under the Born-Markov and the rotating-wave approximations while renormalizing to the resonance frequency of the TLS, the Hamiltonian for this system is ($\hbar = v_g = 1$)

$$\hat{H} = -i \int_{\mathbb{R}} dx \hat{a}^\dagger(x) \partial_x \hat{a}(x) + \sqrt{\Gamma} [\hat{a}^\dagger(x_1) \hat{\sigma}_- + \hat{\sigma}_+ \hat{a}(x_1)] + \hat{H}_{\text{in}}(t) + \hat{H}_{\text{cap}}(t), \quad (\text{S43})$$

where $\hat{a}^\dagger(x)$ [$\hat{a}(x)$] is the photon creation (annihilation) operator at position x , satisfying the commutation relation $[\hat{a}(x), \hat{a}^\dagger(x')] = \delta(x - x')$; and $\hat{\sigma}_\pm$ are the Pauli operators of the TLS. The first term in the Hamiltonian describes the right-propagating photon field while the second term describes the interaction between the TLS and the photon field at position x_1 with coupling strength Γ [4, 5]. To include a general input photon state and to analyze a specific mode in the photon field, we include two Hamiltonians with dynamical coupling strengths, responsible for the release and capture of modes with complex wave packets $u(t)$ and $v(t)$ into and out of the waveguide [6]; $\hat{H}_{\text{in}}(t) = g_u^*(t) \hat{a}^\dagger(x_0) \hat{c}_{\text{in}} + g_u(t) \hat{c}_{\text{in}}^\dagger \hat{a}(x_0)$ and $\hat{H}_{\text{cap}}(t) = g_v^*(t) \hat{a}^\dagger(x_2) \hat{c}_{\text{cap}} + g_v(t) \hat{c}_{\text{cap}}^\dagger \hat{a}(x_2)$, where $\hat{c}_{\text{in}}^\dagger$ (\hat{c}_{in}) and $\hat{c}_{\text{cap}}^\dagger$ (\hat{c}_{cap}) are the excitation creation (annihilation) operators for the input and capture virtual cavities, respectively.

The full Hamiltonian of Eq. (S43) describes a cascaded system where vacuum field sequentially interacts with the input cavity, the TLS and the capture cavity, i.e. the corresponding positions satisfy $x_0 < x_1 < x_2$. Here, we proceed to an interaction frame with respect to the right-propagating photon field in absence of the chiral atom, this is equivalent to transforming argument of the photon field operators to $\hat{a}(x) \rightarrow \hat{a}(x - t)$. Now we can label the photon field operators using t , and they satisfy the commutation relation $[\hat{a}(t), \hat{a}^\dagger(t')] = \delta(t - t')$. We emphasize that this commutation relation is the result of taking $v_g = 1$ and going into the interaction frame, and should not be confused with that of the Heisenberg picture. Consequently, a right-propagating mode creation operator for a normalized complex wave packet $u(t)$ reads

$$\hat{a}_u^\dagger = \int_0^\infty dt u(t) \hat{a}^\dagger(-t). \quad (\text{S44})$$

The time dependent coupling strength is chosen as,

$$g_u(t) = \frac{-iu^*(t)}{\sqrt{1 - \int_0^t dt' |u(t')|^2}}, \quad (\text{S45})$$

such that the input cavity initialized at $t = 0$ will asymptotically release a specific state into the waveguide in a temporal mode $u(t)$ [6–8]. Similarly, the capture cavity will asymptotically capture photons in a temporal mode $v(t)$ if the coupling strength is chosen to be [9]

$$g_v(t) = \frac{iv^*(t)}{\sqrt{\int_0^t dt' |v(t')|^2}}. \quad (\text{S46})$$

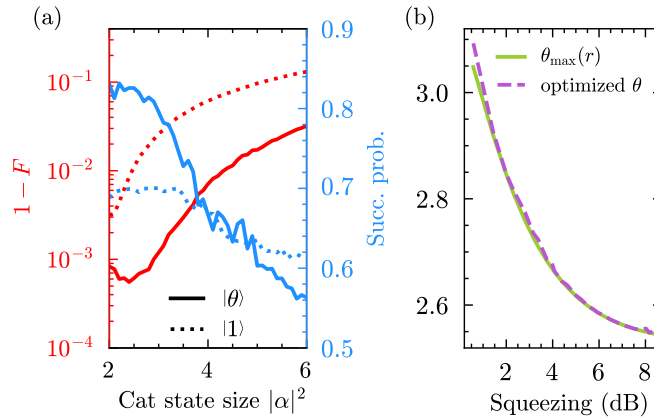


FIG. S5. (a) The infidelity (red) and the success probability (blue) using the nonlinear photon subtraction protocol; the squeezed θ states (solid) and the squeezed single-photon states (dotted) as inputs. (b) $\theta_{\max}(r)$ (solid green) and optimized θ (dashed purple) against the initial squeezing strength.

The dynamics of the photon field and performing photon-subtraction of the nonlinear protocol is described as follows. At $t = 0$, the input cavity is prepared in the state $|r, \theta_{\max}\rangle$. Releasing the resource state into a Gaussian mode $u(t) = \frac{1}{\sqrt{\sigma\pi^{1/4}}}e^{-(t-t_0)^2/2\sigma^2}$ of width σ , is generated by the interactions between the input cavity and the vacuum field. The many-photon cavity interaction is modeled numerically by solving a quantum stochastic Schrödinger equation using the matrix product state (MPS) description, explained in the next section. In terms of the mode creation operators, the state of the photon field is

$$\sum_{n=0} B_n(r, \theta_{\max}) \frac{\hat{a}_u^{\dagger 2n}}{\sqrt{(2n)!}} |0\rangle, \quad (\text{S47})$$

where $B_n(r, \theta)$ are defined by Eq. (S30). After scattering with the TLS (i.e. for a sufficient long time, the input cavity and the TLS both reach their ground states), we calculate the first-order coherence $G^{(1)}(t, t') = \langle \hat{a}^\dagger(t)\hat{a}(t') \rangle = \sum_i \bar{n}_i v_i^*(t)v_i(t')$ and diagonalizing it to find the dominant mode $v_1(t)$, where $\bar{n}_1 \geq \bar{n}_i$ for all i . We extract the dominant mode $v_1(t)$ using a virtual cavity by choosing $g_{v_1}(t)$ according to Eq. (S46). To achieve maximum fidelity, i.e. maximum overlap with a pure target state, one must also maximize the purity of the prepared state. But now, the non-dominant modes are entangled with the virtual cavity, and the purification is performed via a single-photon subtraction by tracing over all single-photon detection events across all possible detection times (i.e. projecting onto the single-photon sector). The output state collected by the virtual cavity is generally entangled with the multi-mode output photon field. For example, for two modes (a dominant mode in the cavity and an ancillary mode in the field), then upon projective measurement on the ancillary mode, the purity of the state in the dominant mode would be unity.

We adapt a gradient-descent optimization algorithm [10] to optimize the squeezing strength and the wave packet width for maximum fidelity against a given cat state of size $|\alpha|^2$. Indeed, the optimized output state is approximately occupied by two modes, $(\bar{n}_1 + \bar{n}_2)/\sum_i \bar{n}_i \sim 0.95$, depending on the squeezing strength. Furthermore, in Fig. S5(b) we show that $\theta_{\max}(r)$ matches the optimized θ if it was included as an optimization parameter.

In Fig. S5(a) we compare the performance of the squeezed θ states and the squeezed single-photon states as inputs. The θ states have an order of magnitude smaller infidelities and much higher success probabilities for generating cat state of size $|\alpha|^2 \leq 4$. Additionally, the single photons require approximately 10 dB of squeezing to generate cat state of size $|\alpha|^2 \approx 2$. In Fig. S6, we showcase the fidelity and success probability in parameter space (squeezing strength and wave packet width) for the squeezed θ states and single-photons. Particularly, in Fig. S6(d), the success probability of detecting a photon in the non-dominant mode exhibits a jump at approximately 4 dB of initial squeezing. From Fig. S1(b), the mean photon number of the 4 dB squeezed single-photon state is approximately 2. The interpretation is that, the non-dominant modes need to have sufficient amplitude over the single-photon sector for single-photon subtraction to have high success probability.

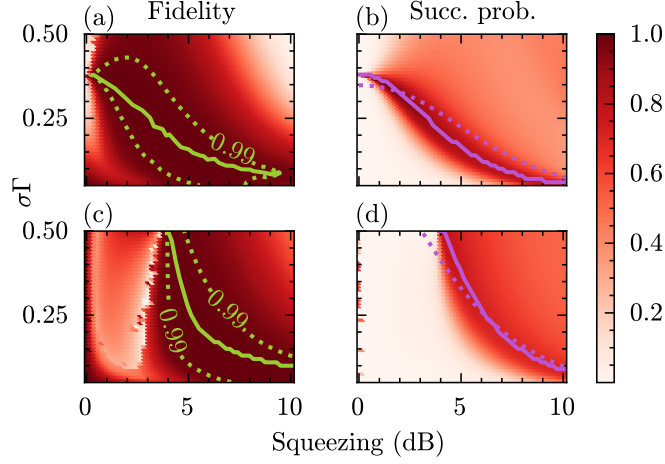


FIG. S6. The fidelity (first column) and the success probability (second column) for using the θ states (first row) and single-photon (second row) as inputs for the nonlinear photon subtraction protocol. In all panels, the input states are subject to initial squeezing strength up to 10 dB and are released into the waveguide in a Gaussian wave packet of width σ . Moreover, the highest fidelity (success probability) across all squeezing strengths is highlighted by the solid green (purple) line. In (a) and (c), the region with fidelity $F > 0.99$ is enclosed by the dotted green contour. In (b) and (d), the π -pulse estimation is given by the dotted purple line.

A. Matrix product state description

Here we adapt the matrix product state (MPS) description for solving the quantum stochastic Schrödinger equation [11–17] and calculating the first-order coherence and performing single-photon detection on the photon field. We begin by writing down the solution to the the quantum stochastic Schrödinger equation, followed by approximating the total time evolution by a product of first-order-trotter-decomposed unitary operators on a discretized photon field. Finally, we represent dynamics of the entire system and the photon field in the MPS formalism. We start by defining the quantum Wiener process

$$B(t) = \int_0^t dt' \hat{a}(-t'). \quad (\text{S48})$$

With $dB(t) = B(t + dt) - B(t)$, the quantum stochastic Schrödinger equation is

$$d\hat{U}(t) = -i[g_u^*(t)dB^\dagger(t - x_0)\hat{c}_{\text{in}} + \sqrt{\Gamma}dB^\dagger(t - x_1)\hat{\sigma}_- + g_v^*(t)dB^\dagger(t - x_2)\hat{c}_{\text{cap}} + \text{h.c.}]\hat{U}(t), \quad (\text{S49})$$

with the solution

$$\hat{U}(t, 0) = \mathcal{T} \exp \left\{ -i \int_0^t [g_u^*(t')dB^\dagger(t' - x_0)\hat{c}_{\text{in}} + \sqrt{\Gamma}dB^\dagger(t' - x_1)\hat{\sigma}_- + g_v^*(t')dB^\dagger(t' - x_2)\hat{c}_{\text{cap}} + \text{h.c.}] \right\}, \quad (\text{S50})$$

where \mathcal{T} denotes the time-ordered exponential. Discretizing the photon field into time bins of width Δt and defining the quantum noise increments as

$$\Delta B(t_k) = B((k+1)\Delta t) - B(k\Delta t) = \int_{k\Delta t}^{(k+1)\Delta t} dt \hat{a}(-t), \quad (\text{S51})$$

and they satisfy the commutation relation, $[\Delta B(t_k), \Delta B^\dagger(t_{k'})] = \Delta t \delta_{k,k'}$. These quantum noise increments are related to the ladder operators of each time bin by $\hat{a}_k = \Delta B(t_k)/\sqrt{\Delta t}$, where $[\hat{a}_k, \hat{a}_{k'}^\dagger] = \delta_{k,k'}$. The total time evolution operator can be expressed in steps of Δt

$$\hat{U}(t, 0) = \lim_{N \rightarrow \infty} \hat{U}(t, N\Delta t) \cdots \hat{U}(\Delta t, 0). \quad (\text{S52})$$

This allows us to approximate each evolution time step up to the first order in Δt

$$\hat{U}((k+1)\Delta t, k\Delta t) \approx \exp \left\{ -i [g_u^*(t_k)\Delta B^\dagger(t_k)\hat{c}_{\text{in}} + \sqrt{\Gamma}\Delta B^\dagger(t_{k-1})\hat{\sigma}_- + g_v^*(t_k)\Delta B^\dagger(t_{k-2})\hat{c}_{\text{cap}} + \text{h.c.}] \right\}, \quad (\text{S53})$$

$$= \hat{U}_{k,\text{cap}} \hat{U}_{k,\text{TLS}} \hat{U}_{k,\text{in}}, \quad (\text{S54})$$

since the input photon bath and the capture cavity are in vacuum and the TLS is in the ground state, we have conveniently defined $x_0 = 0, x_1 = \Delta t, x_2 = 2\Delta t$.

The physical interpretation of this unitary is that, the input field (time bin) of the TLS is the output field (time bin) of the input cavity and similarly for the capture cavity and the TLS. In other words, this unitary describes a cascaded system. We can express the unitary as a product of three two-body local unitary operators because each part of the system are coupled to different time bins. Finally, the total time evolution of the entire system and the photon field is generated by applying these unitary operators in a time-ordered fashion.

Let us now introduce the MPS description of the systems and the time bins representation of the photon field. Initially, the time bins are all in vacuum, the input cavity is in the resource state $|r, \theta_{\max}\rangle$, the TLS is in the ground state and the capture cavity is in vacuum, i.e.

$$|\psi(0)\rangle = |0\rangle^{\otimes N} |r, \theta_{\max}\rangle_{\text{in}} |g\rangle_{\text{TLS}} |0\rangle_{\text{cap}}. \quad (\text{S55})$$

However, a general state of the system and time bins is

$$|\psi\rangle = \sum_{\{i_n, \dots, i_0, s_{\text{in}}, s_{\text{TLS}}, s_{\text{cap}}\}} \psi_{i_n, \dots, i_0, s_{\text{in}}, s_{\text{TLS}}, s_{\text{cap}}} |i_n, \dots, i_0, s_{\text{in}}, s_{\text{TLS}}, s_{\text{cap}}\rangle, \quad (\text{S56})$$

where $|i_k\rangle = \Delta B^{\dagger i_k}(t_k) / \sqrt{\Delta^{i_k} i_k!} |0\rangle_{t_k}$, is the number state of the k -th time bin, and $|s_{\text{in}}, s_{\text{TLS}}, s_{\text{cap}}\rangle$ are the states of the system (the cavities and the TLS), $\psi_{i_n, \dots, i_0, s_{\text{in}}, s_{\text{TLS}}, s_{\text{cap}}}$ is the wavefunction and $\{i_n, \dots, i_0, s_{\text{in}}, s_{\text{TLS}}, s_{\text{cap}}\}$ denotes summing over all configurations. The underlying Hilbert space grows exponentially and is infeasible to track a general state. Here, we adapt the MPS approximation to the wavefunction

$$|\psi\rangle \approx \sum_{\{i_n, \dots, i_0, s_{\text{in}}, s_{\text{TLS}}, s_{\text{cap}}\}} A[i_n] \cdots A[i_0] A[s_{\text{in}}] A[s_{\text{TLS}}] A[s_{\text{cap}}] |i_n, \dots, i_0, s_{\text{in}}, s_{\text{TLS}}, s_{\text{cap}}\rangle, \quad (\text{S57})$$

where each $A[i_k]$ of the physical index i_k , is a matrix of size $D_{i_{k+1}} \times D_{i_k}$ representing the wavefunction of the k -th time bin. Similarly, the system matrices are adjacent to each other forming the matrix product $A[s_{\text{in}}] A[s_{\text{TLS}}] A[s_{\text{cap}}]$. Hence, including the physical index, each $A[i_k]$ is a rank-3 tensor. At first sight, the advantages of adapting the MPS ansatz is not apparent. However, we can restrict the number of excitations in each time bin to only have a few photons (≤ 2), which is appropriate in the limit of $\Gamma\Delta t \ll 1$. Subsequently, reducing the physical dimension of each tensor. Observe that these time bin matrices are intrinsically timely ordered, labeled by the time when they interact with the input cavity, $k\Delta t$. Further, the system matrices are also ordered by the time which they interact with the 0-th time bin. We note that, the MPS structure with embedded time ordering product of the matrices give rise to a natural extension to the continuous matrix product state (cMPS) by taking $\Delta t \rightarrow 0$ [18–20].

Time evolution to the next time step is generated by applying a slightly modified unitary operator of Eq. (S54)

$$\hat{U}'_0 |\psi(t_0)\rangle = |\psi(t_1)\rangle = \sum_{\{i_n, \dots, i_0, s_{\text{in}}, s_{\text{TLS}}, s_{\text{cap}}\}} A[i_n] \cdots A[i_1] A[s_{\text{in}}] A[s_{\text{TLS}}] A[s_{\text{cap}}] A[i_0] |i_n, \dots, i_0, s_{\text{in}}, s_{\text{TLS}}, s_{\text{cap}}\rangle, \quad (\text{S58})$$

where $\hat{U}'_0 = \hat{V}_{\text{swap}} \hat{U}_{0, \text{cap}} \hat{V}_{\text{swap}} \hat{U}_{0, \text{TLS}} \hat{V}_{\text{swap}} \hat{U}_{0, \text{in}}$, these swap operators swap the ordering of the matrices of the interacting parties such that the following unitary is a local two-body unitary, i.e. $A'''[i_0] A'[s_{\text{in}}] A'[s_{\text{TLS}}] A'[s_{\text{cap}}] \rightarrow A[s_{\text{in}}] A''[i_0] A'[s_{\text{TLS}}] A'[s_{\text{cap}}] \rightarrow A[s_{\text{in}}] A[s_{\text{TLS}}] A'[i_0] A'[s_{\text{cap}}] \rightarrow A[s_{\text{in}}] A[s_{\text{TLS}}] A[s_{\text{cap}}] A[i_0]$. After applying each unitary and swap operator, the two-site tensor is factorized using singular value decomposition (SVD) into matrices satisfying the form given by Eq. (S57). Notice, we have omitted the time bins $A[i_{-1}]$ and $A[i_{-2}]$, since the these time bins and the capture cavity are in vacuum and the TLS is in the ground state, the interaction between these are trivial. Furthermore, the time bin widths should be chosen such that $\Gamma\Delta t \ll 1$ and consequently the total time evolution should be complete, i.e. there should be sufficient number of time bins (tensors) such that the input cavity and the TLS are in their ground states and the capture cavity decouples from the time bins. A diagrammatic example of the time evolution is given in Fig. S7.

We have calculated the matrix-product operator representation of the TLS unitary analytically,

$$\hat{U}_{k, \text{TLS}} = \begin{pmatrix} -i\sqrt{\Gamma}\Delta B(t_k) \text{sinc}[\sqrt{\Gamma\Delta t\Delta\Lambda}(t_k)] \\ -i\sqrt{\Gamma} \text{sinc}[\sqrt{\Gamma\Delta t\Delta\Lambda}(t_k)] \Delta B^\dagger(t_k) \\ \cos[\sqrt{\Gamma\Delta t(\Delta\Lambda(t_k) + 1)}] \\ \cos[\sqrt{\Gamma\Delta t\Delta\Lambda}(t_k)] \end{pmatrix}^T \begin{pmatrix} \hat{\sigma}_+ \\ \hat{\sigma}_- \\ |e\rangle \langle e| \\ |g\rangle \langle g| \end{pmatrix}, \quad (\text{S59})$$

where $\Delta\Lambda(t_k) = \int_{t_k}^{t_{k+1}} dt \hat{a}^\dagger(-t) \hat{a}(-t) = \hat{n}_k$ is the photon number operator of the k -th time bin and T denotes transpose. In practice, having the unitary operators in the exponential form is sufficient.

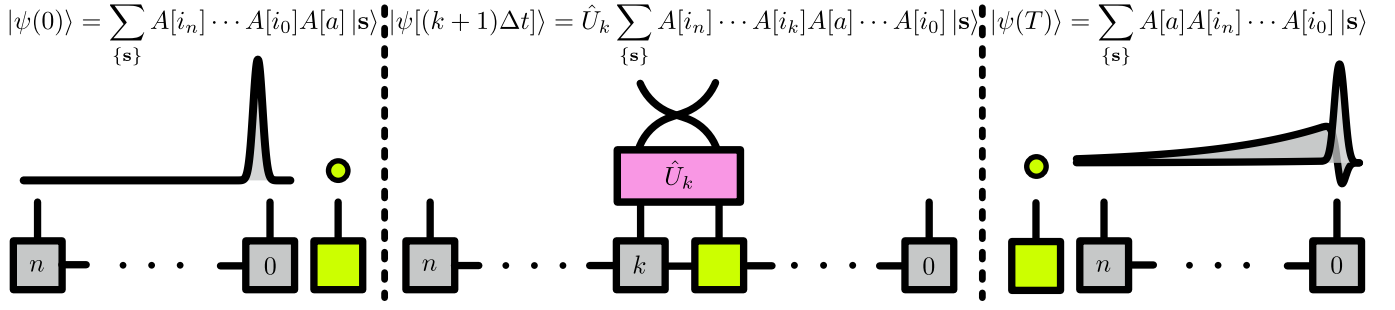


FIG. S7. Diagrammatic representation of the time evolution of the system. In the left panel, at the initial time, the field is in the discretized state described by Eq. (S47) contained in a Gaussian wave packet and the TLS is in its ground state. The time bins are represented by the grey blocks, labeled by the order of which they interact with the TLS (represented by the green block). Moreover, these blocks correspond to the matrices in the MPS (equation above) and the matrix and physical indices are represented by the horizontal and vertical “legs” attached to each block, respectively. Hence, matrix multiplication is represented by joining the horizontal “legs” together. The middle panel depicts time evolution by updating the TLS matrix and the adjacent time bin matrix using the unitary operator defined by Eq. (S59). Performing SVD after swapping the corresponding physical indices of the time bin and TLS factorizes the entire state back to the MPS form and it is now ready for evolution to the next time step. For a sufficient long time, in the last panel, the TLS returns to its ground state and the field is now in a multi-mode state.

The maximum bond dimension, defined as $\chi_{\max} = \max_{i_k} (D_{i_k})$, characterizes the numerical difficulty of implementing these MPSs. Initially, the MPS description is exact up to the truncation of the input cavity Hilbert space, and the maximum bond dimension is $\chi_{\max} = 1$. At total time evolution, and without any truncation of small singular values, the maximum bond dimension is $\chi_{\max} =$ the Hilbert space dimension of the system (the cavities and TLS), in practice, we set a cut-off (10^{-7}) to truncate the small singular values to improve the runtime cost. When truncating, one should set the orthogonality center to either one of the adjacent matrices such that the singular values are the Schmidt coefficients of the state decomposed in the bipartite subspaces. We chose $\Gamma\Delta t = 0.005$ and 2000 time bins.

We calculate two observables from the photon field, namely, the first-order coherence $G^{(1)}(t, t') = \langle \hat{a}^\dagger(t) \hat{a}(t') \rangle$ and projective measurements onto the single-photon sector. In the time bin representation, the field operators are mapped by $\hat{a}(t_k) \rightarrow \Delta B(t_k)/\Delta t$, hence the first-order coherence is $G^{(1)}(t_k, t_{k'}) = \langle \Delta B^\dagger(t_k) \Delta B(t_{k'}) \rangle / \Delta t^2$. The unnormalized density matrix after tracing over all single-photon detection times is $\hat{\rho} = \text{Tr}_s \sum_k \langle 1_k | \text{out} \rangle \langle \text{out} | 1_k \rangle$, where $|1_k\rangle$ denotes the product state with $|1\rangle$ in the k -th time bin and vacuum in all other time bins, Tr_s denotes tracing over the system. Ultimately, we numerically simulated the MPS description of the dynamics using the `JULIA` package `ITensors.jl` [21].

IV. DETERMINISTIC θ STATE GENERATION

Here we provide further details on the deterministic generation of θ states using two three-level atoms coupled to a cavity. The cavity is then coupled to a one-dimensional continuum of modes. The three-level atoms have ground states $|g\rangle$, shelving state $|s\rangle$, and an optically excited state $|e\rangle$. This is shown in the schematic Fig. S8(a). Let us take the ground and shelving states to be at zero energy. The Hamiltonian for the entire system is ($\hbar = v_g = 1$),

$$\hat{H} = \omega_0 [\hat{\sigma}_+^1 \hat{\sigma}_-^1 + \hat{\sigma}_+^2 \hat{\sigma}_-^2] + \omega_c \hat{c}^\dagger \hat{c} + \int dx \hat{a}^\dagger(x) [\tilde{\omega} - i\partial_x] \hat{a}(x) \quad (\text{S60})$$

$$- i\sqrt{\kappa} [\hat{a}^\dagger(0) \hat{c} - \hat{c}^\dagger \hat{a}(0)] + g [(\hat{\sigma}_+^1 + \hat{\sigma}_+^2) \hat{c} + \hat{c}^\dagger (\hat{\sigma}_-^1 + \hat{\sigma}_-^2)]. \quad (\text{S61})$$

Here σ_-^i (σ_+^i) are the lowering (raising) operator for the $|g\rangle$ - $|e\rangle$ transition of atom $i = 1, 2$, \hat{c} (\hat{c}^\dagger) is the cavity annihilation (creation) operator and $\hat{a}(x)$ ($\hat{a}^\dagger(x)$) is the channel annihilation (creation) operator at position x . We also have κ as the cavity-channel decay rate, g is the atom-cavity coupling rate and ω_0 is the atomic optical resonance frequency, ω_c is the cavity resonance frequency, and $\tilde{\omega}$ is the frequency about which we linearise the dispersion of the channel.

Let us consider the atoms to be on resonance with the cavity and that the one-dimensional photon modes are linearised about this frequency, i.e., $\omega_0 = \omega_c = \tilde{\omega}$. Moving into an interaction picture with respect to the Hamiltonian

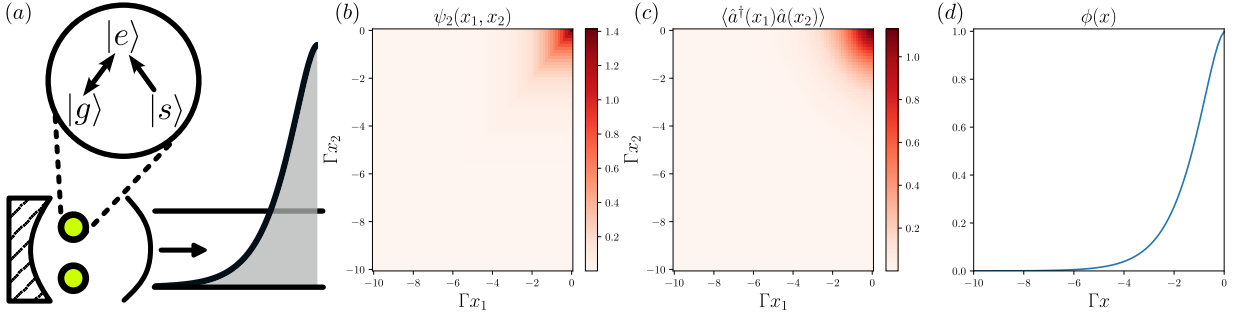


FIG. S8. Deterministic θ state generation using two three-level atoms coupled to a cavity. (a) Schematic showing three-level atoms each with ground state $|g\rangle$, excited state $|e\rangle$ and shelving state $|s\rangle$ coupled to a single-sided cavity. Photons emitted from the atoms couple to the cavity which is itself coupled to a collection mode. (b) Two-photon wavefunction $\psi_2(x_1, x_2)$ of a two-excitation superradiant state. (c) First-order correlation function $\langle \hat{a}^\dagger(x_1)\hat{a}(x_2) \rangle$ of the two-photon superradiant state. (d) Eigenvector $\phi(x)$ corresponding to the largest eigenvalue of $\langle \hat{a}^\dagger(x_1)\hat{a}(x_2) \rangle$.

$\hat{H}_0 = \omega_0[\sigma_+^1\sigma_-^1 + \sigma_+^2\sigma_-^2 + \hat{c}^\dagger\hat{c} + \int dx \hat{a}^\dagger(x)\hat{a}(x)]$, we have the interaction Hamiltonian in the interaction picture,

$$\hat{H}_I = -i \int dx \hat{a}^\dagger \partial_x \hat{a}(x) - i\sqrt{\kappa} [\hat{a}^\dagger(0)\hat{c} - \hat{c}^\dagger\hat{a}(0)] + g [(\hat{\sigma}_+^1 + \hat{\sigma}_+^2)\hat{c} + \hat{c}^\dagger(\hat{\sigma}_-^1 + \hat{\sigma}_-^2)]. \quad (\text{S62})$$

The equations of motion for the photon channel and cavity operators are,

$$i\partial_t \hat{a}(x, t) = -i\partial_x \hat{a}(x, t) - i\sqrt{\kappa}\delta(x)\hat{c}(t), \quad (\text{S63})$$

$$i\partial_t \hat{c}(t) = i\sqrt{\kappa}\hat{a}(0) + g(\hat{\sigma}_-^1 + \hat{\sigma}_-^2), \quad (\text{S64})$$

Solving for the channel operators we have,

$$\hat{a}(x, t) = \hat{a}(x - t, 0) - \sqrt{\kappa}\hat{c}(t - x)\theta(x)\theta(t - x). \quad (\text{S65})$$

Using this solution, the differential equation for the cavity operator becomes

$$i\partial_t \hat{c}(t) = i\sqrt{\kappa} \left[\hat{a}_{\text{in}}(t) - \frac{\sqrt{\kappa}}{2}\hat{c}(t) \right] + g(\hat{\sigma}_-^1 + \hat{\sigma}_-^2), \quad (\text{S66})$$

where we have defined $\hat{a}_{\text{in}}(t) = \hat{a}(-t, 0)$. We now consider the system in the bad-cavity limit where $\kappa \gg g$. In this limit the cavity can be adiabatically eliminated and $\partial_t \hat{c}(t) \sim 0$. This allows making the approximation

$$\hat{c}(t) \sim \frac{\sqrt{\kappa}\hat{a}_{\text{in}}(t) - ig(\hat{\sigma}_-^1 + \hat{\sigma}_-^2)}{\kappa/2}. \quad (\text{S67})$$

Let us now consider a system operator \hat{s} , where \hat{s} can be any operator for atom 1 and/or 2. Using the result from the adiabatic elimination of the cavity, \hat{s} obeys the equation of motion,

$$i\partial_t \hat{s}(t) = g [[\hat{s}, \hat{\sigma}_+^1 + \hat{\sigma}_+^2] \hat{c} + \hat{c}^\dagger [\hat{s}, \hat{\sigma}_-^1 + \hat{\sigma}_-^2]] \quad (\text{S68})$$

$$i\partial_t \hat{s}(t) \sim \frac{2g}{\sqrt{\kappa}} [[\hat{s}, \hat{\sigma}_+^1 + \hat{\sigma}_+^2] [\hat{a}_{\text{in}}(t) - ig(\hat{\sigma}_-^1 + \hat{\sigma}_-^2)] + [\hat{a}_{\text{in}}^\dagger(t) + ig(\hat{\sigma}_+^1 + \hat{\sigma}_+^2)] [\hat{s}, \hat{\sigma}_-^1 + \hat{\sigma}_-^2]]. \quad (\text{S69})$$

This evolution equation can arise from an effective Hamiltonian,

$$\hat{H}_{\text{eff}} = -i \int dx \hat{a}^\dagger(x) \partial_x \hat{a}(x) + \sqrt{\Gamma} [\hat{a}^\dagger(0)(\hat{\sigma}_-^1 + \hat{\sigma}_-^2) + (\hat{\sigma}_+^1 + \hat{\sigma}_+^2)\hat{a}(0)]. \quad (\text{S70})$$

After adiabatic elimination of the cavity, we obtain an effective evolution under a Hamiltonian where the atom directly couples to the one-dimensional channel with an effective decay rate of $\Gamma = 4g^2/\kappa$.

To find the two-photon superradiant state we solve for the dynamics of the system under the effective Hamiltonian for the initial condition that the two atoms are initially in the excited state $|ee\rangle$. The superradiance problem is

exactly solvable for N atoms [22]. Here we provide the two-atom two-excitation solution. To do this we write the entire wavefunction of the system using a two-excitation ansatz,

$$|\psi(t)\rangle = \left[\frac{1}{\sqrt{2}} \int dx_1 dx_2 \hat{a}^\dagger(x_1) \hat{a}^\dagger(x_2) \alpha(x_1, x_2, t) + \int dx \hat{a}^\dagger(x) \hat{\sigma}_+^1 p_1(x, t) + \int dx \hat{a}^\dagger(x) \hat{\sigma}_+^2 p_2(x, t) |0\rangle + s(t) \hat{\sigma}_+^1 \hat{\sigma}_+^2 \right] |0\rangle. \quad (\text{S71})$$

Here $|0\rangle$ indicates both atoms in the ground state and all modes of the photon continuum in vacuum. Note that the effective Hamiltonian is permutationally invariant under exchange of the atom indices $1 \leftrightarrow 2$. This means that $p_1(x, t) = p_2(x, t) \equiv p(x, t)$. From this ansatz we have the equations of motion,

$$i\partial_t \alpha(x_1, x_2, t) = -i[\partial_{x_1} + \partial_{x_2}] \alpha(x_1, x_2, t) + \sqrt{2\Gamma} [\delta(x_1) p(x_2, t) + \delta(x_2) p(x_1, t)], \quad (\text{S72})$$

$$i\partial_t p(x, t) = -i\partial_x p(x, t) + \sqrt{\Gamma} \delta(x) s(t) + \sqrt{\frac{\Gamma}{2}} [\alpha(0, x, t) + \alpha(x, 0, t)], \quad (\text{S73})$$

$$i\partial_t s(t) = 2\sqrt{\Gamma} p(0, t), \quad (\text{S74})$$

with the initial condition $p(x, 0) = \alpha(x_1, x_2, 0) = 0$ and $s(0) = 1$. By integrating (S72) and (S74) over the origin we obtain relations, $p(0^+, t) = -i\sqrt{\Gamma} s(t)$ and $\alpha(0^+, x, t) = -i\sqrt{2\Gamma} p(x, t)$. To obtain these we have used the definition $f(0) = [f(0^+) + f(0^-)]/2$ and the fact that the fields vanish for $x < 0$. Using these we can easily solve the third equation and obtain,

$$s(t) = e^{-\Gamma t}. \quad (\text{S75})$$

To solve the equation for $p(x, t)$ we introduce comoving coordinates $\xi = x - t$ and $\eta = t$ and use the relation $\alpha(0^+, x, t) = -i\sqrt{2\Gamma} p(x, t)$. Formally integrating the equation gives,

$$p(\xi, \eta) = -i\sqrt{\Gamma} e^{-\Gamma(\xi+\eta)} s(-\xi) \theta(-\xi) \theta(\eta + \xi) = -i\sqrt{\Gamma} e^{-\Gamma\eta} \theta(-\xi) \theta(\eta + \xi). \quad (\text{S76})$$

Finally, to solve for $\alpha(x_1, x_2, t)$ we again use comoving coordinates, $\xi_1 = x_1 - t$, $\xi_2 = x_2 - t$, $\eta = t$. After this transformation the equation can again be solved by integration giving,

$$\alpha(\xi_1, \xi_2, \eta) = -i\sqrt{2\Gamma} [p(\xi_1, -\xi_2) \theta(-\xi_2) \theta(\xi_2 + \eta) + p(\xi_2, -\xi_1) \theta(-\xi_1) \theta(\xi_1 + \eta)]. \quad (\text{S77})$$

In the $t \rightarrow \infty$ limit the atom has completely decayed and the entire photon wavefunction is away from $x = 0$. Using comoving coordinates we define a two-photon wavefunction obtained from the two-excitation superradiant decay,

$$|\bar{2}\rangle = \frac{1}{\sqrt{2}} \int dx_1 dx_2 \hat{a}^\dagger(x_1) \hat{a}^\dagger(x_2) |0\rangle \psi(x_1, x_2), \quad (\text{S78})$$

with

$$\psi(x_1, x_2) = \theta(-x_1) \theta(-x_2) [e^{\Gamma x_2} \theta(x_1 - x_2) + e^{\Gamma x_1} \theta(x_2 - x_1)]. \quad (\text{S79})$$

The wavefunction is plotted in Fig. S8(b). In the main text, the wavefunction is given in the $x_1 > x_2$ subspace.

A. Calculating the fidelity of the superradiant state

Using superradiant emission to make θ state produces the state defined in the main text as,

$$|\bar{\theta}\rangle = \cos(\theta/2) |0\rangle + \sin(\theta/2) |\bar{2}\rangle. \quad (\text{S80})$$

We wish to compute the fidelity of this state with the ideal θ state, i.e., $F = |\langle \theta | \bar{\theta} \rangle|^2$. Since the photon in the ideal theta state can be in any mode, we can calculate this overlap by decomposing $|\bar{2}\rangle$ into an orthogonal basis and choosing the dominant mode. There are two equivalent ways to do this, using the Takagi decomposition of the two-photon wavefunction $\psi(x_1, x_2)$ or by diagonalising the first-order coherence function $\langle \hat{a}^\dagger(x_1) \hat{a}(x_2) \rangle$ of the two-photon wavefunction. We choose the latter. The first-order correlation function of the two-photon state is,

$$\langle \hat{a}^\dagger(x_1) \hat{a}(x_2) \rangle = \int dx \psi^*(x_1, x) \psi(x, x_2). \quad (\text{S81})$$

This is plotted in Fig. S8(c). Considering x_1 and x_2 as discrete variables, the first-order coherence function forms a Hermitian matrix whose eigenvectors give an orthonormal basis on which $\psi(x_1, x_2)$ can be represented. The eigenvector with the largest eigenvalues gives the dominant mode which we call $\phi(x)$, which is plotted in Fig. S8(d). We then have

$$\langle 2|\bar{2}\rangle = \int dx_1 dx_2 \psi^*(x_1, x_2) \phi(x_1) \phi(x_2) \quad (\text{S82})$$

We find that for the superradiant state the value is $\langle 2|\bar{2}\rangle = 0.954$. This then gives the overlap

$$F = |\langle \theta|\bar{\theta}\rangle|^2 = |\cos^2(\theta/2) + \sin^2(\theta/2) \langle 2|\bar{2}\rangle|^2 = 1 - 2 \sin^2(\theta/2) \text{Re}[1 - \langle 2|\bar{2}\rangle] + 4 \sin^4 \theta/2 |1 - \langle 2|\bar{2}\rangle|^2 \quad (\text{S83})$$

$$\sim 1 - 2 \sin^2(\theta/2) \times 0.046. \quad (\text{S84})$$

B. Including loss in superradiant decay

Here we calculate the effect of imperfect coupling of the atoms to the one-dimensional channel on the fidelity of the θ states. We do this by considering a worst-case scenario where the loss is a fraction of the superradiant decay. To do this we add an additional channel of modes with coupling coefficient γ in the effective Hamiltonian,

$$\hat{H}_{\text{eff}} = -i \int dx \hat{a}^\dagger(x) \partial_x \hat{a}(x) - i \int dx \hat{b}^\dagger(x) \partial_x \hat{b}(x) + \sqrt{\Gamma} [\hat{a}^\dagger(0)(\hat{\sigma}_-^1 + \hat{\sigma}_-^2) + (\hat{\sigma}_+^1 + \hat{\sigma}_+^2) \hat{a}(0)] \quad (\text{S85})$$

$$+ \sqrt{\gamma} [\hat{b}^\dagger(0)(\hat{\sigma}_-^1 + \hat{\sigma}_-^2) + (\hat{\sigma}_+^1 + \hat{\sigma}_+^2) \hat{b}(0)]. \quad (\text{S86})$$

We now define new operators,

$$\hat{a}_e(x) = \frac{\sqrt{\Gamma} \hat{a}(x) + \sqrt{\gamma} \hat{b}(x)}{\sqrt{\Gamma + \gamma}} = \sqrt{\beta} \hat{a}(x) + \sqrt{1 - \beta} \hat{b}(x), \quad (\text{S87})$$

$$\hat{a}_o(x) = \frac{\sqrt{\gamma} \hat{a}(x) - \sqrt{\Gamma} \hat{b}(x)}{\sqrt{\Gamma + \gamma}} = \sqrt{1 - \beta} \hat{a}(x) - \sqrt{\beta} \hat{b}(x), \quad (\text{S88})$$

$$(\text{S89})$$

where we have defined the coupling efficiency $\beta = \Gamma/(\Gamma + \gamma)$. Using these operators the effective Hamiltonian becomes

$$\hat{H}_{\text{eff}} = -i \int dx \hat{a}_e^\dagger(x) \partial_x \hat{a}_e(x) - i \int dx \hat{a}_o^\dagger(x) \partial_x \hat{a}_o(x) + \sqrt{\Gamma + \gamma} [\hat{a}_e^\dagger(0)(\hat{\sigma}_-^1 + \hat{\sigma}_-^2) + (\hat{\sigma}_+^1 + \hat{\sigma}_+^2) \hat{a}_e(0)]. \quad (\text{S90})$$

We note that the $\hat{a}_o(x)$ operator does not enter as an interaction term and is decoupled from the system. The effective Hamiltonian is therefore identical to the original one, but with $\Gamma \rightarrow \Gamma + \gamma$ and $\hat{a} \rightarrow \hat{a}_e$. The two-excitation superradiant solution is thus,

$$|\bar{2}\rangle_e = \frac{1}{\sqrt{2}} \int dx_1 dx_2 \hat{a}_e^\dagger(x_1) \hat{a}_e^\dagger(x_2) |0\rangle \psi(x_1, x_2) \quad (\text{S91})$$

$$= \frac{1}{\sqrt{2}} \int dx_1 dx_2 \left[\sqrt{\beta} \hat{a}^\dagger(x_1) + \sqrt{1 - \beta} \hat{b}^\dagger(x_1) \right] \left[\sqrt{\beta} \hat{a}^\dagger(x_2) + \sqrt{1 - \beta} \hat{b}^\dagger(x_2) \right] |0\rangle \psi(x_1, x_2), \quad (\text{S92})$$

with

$$\psi(x_1, x_2) = \theta(-x_1) \theta(-x_2) \left[e^{(\Gamma + \gamma)x_2} \theta(x_1 - x_2) + e^{(\Gamma + \gamma)x_1} \theta(x_2 - x_1) \right]. \quad (\text{S93})$$

The wavefunction therefore has the same shape, but with the effective decay rate scaling with the sum of the decay of the two channels $\Gamma + \gamma$. We can now compute the fidelity as before,

$$F = |\langle \theta|\bar{\theta}\rangle|^2 = |\cos^2(\theta/2) + \sin^2(\theta/2) \langle 2|\bar{2}\rangle_e|^2 = 1 - 2 \sin^2(\theta/2) \text{Re}[1 - \langle 2|\bar{2}\rangle_e] + 4 \sin^4 \theta/2 |1 - \langle 2|\bar{2}\rangle_e|^2 \quad (\text{S94})$$

$$\sim 1 - 2 \sin^2(\theta/2) (1 - 0.954\beta). \quad (\text{S95})$$

Where we assume that the loss is small such that $(1 - \beta) \ll 1$.

[1] S. L. Braunstein and P. van Loock, Quantum information with continuous variables, Rev. Mod. Phys. **77**, 513 (2005).

- [2] K. Takase, J.-i. Yoshikawa, W. Asavanant, M. Endo, and A. Furusawa, Generation of optical schrödinger cat states by generalized photon subtraction, *Phys. Rev. A* **103**, 013710 (2021).
- [3] U. Chabaud, D. Markham, and F. Grosshans, Stellar representation of non-gaussian quantum states, *Phys. Rev. Lett.* **124**, 063605 (2020).
- [4] P. Lodahl, S. Mahmoodian, S. Stobbe, A. Rauschenbeutel, P. Schneeweiss, J. Volz, H. Pichler, and P. Zoller, Chiral quantum optics, *Nature* **541**, 473 (2017).
- [5] S. Mahmoodian, G. Calajó, D. E. Chang, K. Hammerer, and A. S. Sørensen, Dynamics of many-body photon bound states in chiral waveguide qed, *Phys. Rev. X* **10**, 031011 (2020).
- [6] A. H. Kiilerich and K. Mølmer, Input-output theory with quantum pulses, *Phys. Rev. Lett.* **123**, 123604 (2019).
- [7] J. E. Gough and G. Zhang, Generating nonclassical quantum input field states with modulating filters, *EPJ Quantum Technology* **2**, 10.1140/epjqt/s40507-015-0027-z (2015).
- [8] K. M. Gheri, K. Ellinger, T. Pellizzari, and P. Zoller, Photon-wavepackets as flying quantum bits, *Fortschritte der Physik* **46**, 401 (1998).
- [9] H. I. Nurdin, M. R. James, and N. Yamamoto, Perfect single device absorber of arbitrary traveling single photon fields with a tunable coupling parameter: A qsde approach, in *2016 IEEE 55th Conference on Decision and Control (CDC)*, Vol. 16 (IEEE, 2016) p. 2513–2518.
- [10] D. P. Kingma and J. Ba, Adam: A method for stochastic optimization (2017), arXiv:1412.6980 [cs.LG].
- [11] U. Schollwöck, The density-matrix renormalization group in the age of matrix product states, *Annals of Physics* **326**, 96 (2011), january 2011 Special Issue.
- [12] H. Pichler and P. Zoller, Photonic circuits with time delays and quantum feedback, *Phys. Rev. Lett.* **116**, 093601 (2016).
- [13] C. Schön, E. Solano, F. Verstraete, J. I. Cirac, and M. M. Wolf, Sequential generation of entangled multiqubit states, *Phys. Rev. Lett.* **95**, 110503 (2005).
- [14] C. Schön, K. Hammerer, M. M. Wolf, J. I. Cirac, and E. Solano, Sequential generation of matrix-product states in cavity qed, *Phys. Rev. A* **75**, 032311 (2007).
- [15] S. Arranz Regidor, G. Crowder, H. Carmichael, and S. Hughes, Modeling quantum light-matter interactions in waveguide qed with retardation, nonlinear interactions, and a time-delayed feedback: Matrix product states versus a space-discretized waveguide model, *Phys. Rev. Res.* **3**, 023030 (2021).
- [16] A. L. Grimsmo, B. Royer, J. M. Kreikebaum, Y. Ye, K. O’Brien, I. Siddiqi, and A. Blais, Quantum metamaterial for broadband detection of single microwave photons, *Phys. Rev. Appl.* **15**, 034074 (2021).
- [17] C. W. Gardiner and P. Zoller, *Quantum noise : a handbook of Markovian and non-Markovian quantum stochastic methods with applications to quantum optics*, 3rd ed., Springer complexity (Springer, 2004).
- [18] F. Verstraete and J. I. Cirac, Continuous matrix product states for quantum fields, *Phys. Rev. Lett.* **104**, 190405 (2010).
- [19] T. J. Osborne, J. Eisert, and F. Verstraete, Holographic quantum states, *Phys. Rev. Lett.* **105**, 260401 (2010).
- [20] S. Barrett, K. Hammerer, S. Harrison, T. E. Northup, and T. J. Osborne, Simulating quantum fields with cavity qed, *Phys. Rev. Lett.* **110**, 090501 (2013).
- [21] M. Fishman, S. White, and E. Stoudenmire, The itensor software library for tensor network calculations, *SciPost Physics Codebases* 10.21468/scipostphyscodeb.4 (2022).
- [22] V. I. Yudson, Dynamics of integrable quantum systems, *Zh. Eksp. Teor. Fiz* **88**, 1757 (1985).